ACS OMEGA

Article

Cite This: ACS Omega 2019, 4, 10761−10766

http://pubs.acs.org/journal/acsodf

Elucidating Traffic Junction Effects in MFI Zeolite Using Kinetic Monte Carlo Simulations

Rajamani Krishna* and Jasper M. van Baten

Van 't Hoff Institute for Molecular Sciences, University of Amsterdam, Science Park 904, 1098 XH Amsterdam, The Netherlands

Supporting Information

ABSTRACT: Published experimental studies on the diffusion of *n*-butane (*n*C4)/*iso*-butane (*i*C4), *n*-hexane (*n*C6)/2-methylpentane (2MP), and methane/benzene mixtures in MFI zeolite show that the self-diffusivity of the more mobile (linear) alkanes is diminished by about 1−3 orders of magnitude with increasing proportion of the tardier partners (*i*C4, 2MP, benzene) in the mixture. The strong reduction can be rationalized on the basis of the preferential location of the tardier partners *i*C4, 2MP, and benzene at the channel intersections of MFI, serving to slow down the molecular traffic. The primary objective of this article is to investigate, and quantify, such traffic junction effects with the aid of kinetic Monte Carlo (KMC) simulations. The KMC simulations show that the preferential location of branched molecules at the channel intersections can be effectively considered as an intersection blocking with attendant loss of connectivity of the MFI topology. Consequently, both the Maxwell−Stefan (M−S) diffusivity and self-diffusivity for *n*C4 in the *n*C4/*i*C4 mixtures are lowered below that for the unary *n*C4 diffusion by about 2 orders of magnitude. It is also established that such a lowering of the diffusivity of the more mobile partner is distinctly different from the "correlation" effects that generally manifest in the mixture diffusion in microporous materials.

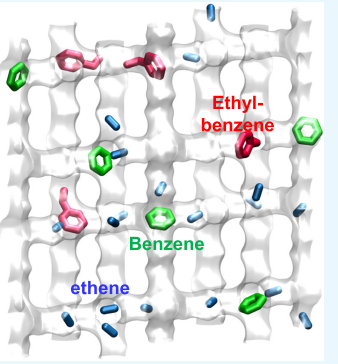

1. INTRODUCTION

MFI (= Mobil FIve) zeolite, also called ZSM-5,[1] is used as a catalyst or adsorbent in a wide variety of industrially important processes such as catalytic cracking, xylene isomerization, alkylation of benzene, and separation of alkane isomers.[2−10] Thin perm-selective layers of MFI zeolite find applications in membrane separations for CO_2 capture.[11−13] MFI has a topology consisting of a set of intersecting straight channels and zigzag (or sinusoidal) channels (see Figure 1a). The channel dimensions are size of 5.5 Å.

A key feature of the mixture diffusion in MFI is that the mobility of any guest constituent is influenced by its partner species. Generally speaking, the mobility of the more mobile species is retarded due to the correlated molecular "jumps" with tardier partner species within the network of intersecting channels of MFI. The proper modeling of such correlation effects is essential in the development and design of industrial process.[14,15]

Mixture diffusion in microporous materials is most commonly modeled using the Maxwell−Stefan (M−S) formulation. For mixtures with two guest constituents, the intracrystalline molar fluxes N_i are related to the chemical potential gradients[14−19]

$$-\rho\frac{\Theta_1}{RT}\frac{d\mu_1}{dz} = \frac{x_2N_1 - x_1N_2}{Đ_{12}} + \frac{N_1}{Đ_1}$$
$$-\rho\frac{\Theta_2}{RT}\frac{d\mu_2}{dz} = \frac{x_1N_2 - x_2N_1}{Đ_{21}} + \frac{N_2}{Đ_2} \quad (1)$$

In eq 1, R is the gas constant, ρ is the framework density, Θ_i are the component loadings expressed in molecules uc^{-1} (uc = unit cell), and x_i are the component mole fractions defined as

$$x_i = \Theta_i/(\Theta_1 + \Theta_2);\ i = 1, 2 \quad (2)$$

The Onsager reciprocal relations impose the symmetry constraint

$$Đ_{12} = Đ_{21} \quad (3)$$

The M−S formulation (eq 1) is phenomenological and serves to define the three diffusivities $Đ_1$, $Đ_2$, and $Đ_{12}$ that characterize binary mixture diffusion. $Đ_1$ and $Đ_2$ characterize the species−wall interactions. The exchange coefficient $Đ_{12}$ quantifies the correlation effects that cause the slowing down of more mobile guest molecules. The degrees of correlations in the molecular jumps within the microporous channels are quantified by the ratios $Đ_1/Đ_{12}$ and $Đ_2/Đ_{12}$. High values of the degrees of correlations imply that the first right-hand members of eq 1 offer significant contributions to the intracrystalline fluxes, causing significant slowing-down effects.[15,20] For $H_2(1)/CO_2(2)$ permeation across the MFI membrane, for example, experimental data[12] are well described by taking $Đ_1/Đ_{12} = 20$.[13,15] In this case, the more strongly adsorbed but tardier CO_2 retards the mobility of the faster-diffusing but poorly adsorbed H_2.

Received: May 12, 2019
Accepted: June 11, 2019
Published: June 20, 2019

DOI: 10.1021/acsomega.9b01369
ACS Omega 2019, 4, 10761−10766

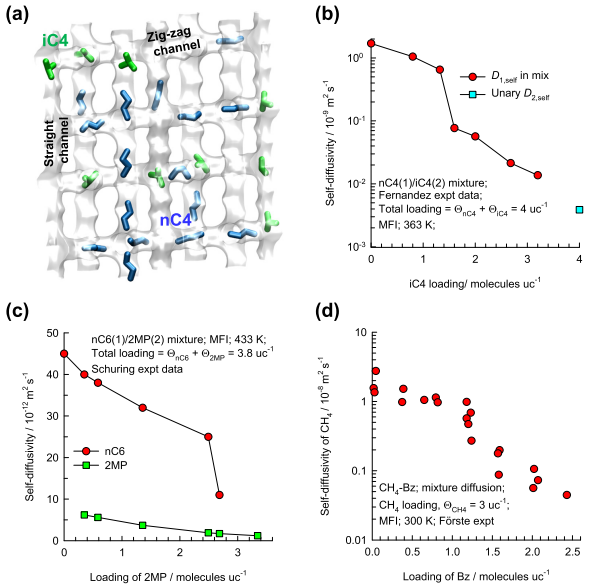

Figure 1. (a) MFI topology with snapshots showing the location of molecules of the *n*C4/*i*C4 mixtures. (b) PFG NMR experimental data of Fernandez et al.[21] on the self-diffusivity of *n*C4 in the *n*C4/*i*C4 mixtures in MFI as a function of the loading of *i*C4. (c) Experimental data of Schuring et al.[22] on self-diffusivities of *n*-hexane (*n*C6) and 2-methylpentane (2MP) as a function of the loading of 2MP. (d) PFG NMR studies of Förste et al.[23] on the self-diffusivity of CH_4 in MFI as function of the loading of the co-adsorbed benzene.

Molecular dynamics (MD) simulations of several binary mixtures in MFI zeolite, and other microporous materials,[19] have established the M−S diffusivities $Đ_1$, and $Đ_2$ can be identified with the corresponding diffusivities for unary systems provided the values are determined at the same pore occupancy θ. The MD simulations also allow quantification of the degrees of correlations, $Đ_1/Đ_{12}$ and $Đ_2/Đ_{12}$.

A special scenario emerges for the mixtures containing branched alkanes and aromatics. Figure 1b presents the PFG NMR data[21] on the self-diffusivities in the binary mixtures of *n*-butane (*n*C4) with *iso*-butane (*i*C4) in which the total loading, $\Theta_t = \Theta_{nC4} + \Theta_{iC4}$, is held constant at 4 molecules uc^{-1}. Increase in the loading of the *i*C4 from $\Theta_{iC4} = 0$ to 2 molecules uc^{-1} has the effect of reducing the self-diffusivity of *n*C4 by about 2 orders of magnitude. As evidenced in the computational snapshot in Figure 1a, the tardier constituent *i*C4 prefers to locate at the channel intersections. The diffusivity of *i*C4 is lower than that of *n*C4 by 3 orders of magnitude. The occupation of some of the intersection sites by *i*C4 may be viewed as effective blockage of the molecular traffic within the channels.

Figure 1c shows the experimental data[22] of the self-diffusivities in the binary mixtures of *n*-hexane (*n*C6) with 2-methylpentane (2MP) in MFI in which the total loading is $\Theta_t = \Theta_{nC6} + \Theta_{2MP} = 3.8$ molecules uc^{-1}. The preferential location of the tardier 2MP at the channel intersections causes a reduction in the self-diffusivity of *n*C6 by about an order of magnitude.

With increase in the loading of benzene (Bz), the self-diffusivity of CH_4 in binary CH_4/Bz mixtures is reduced by about 2 orders of magnitude (see Figure 1d). The explanation is again to be found in the reduction of CH_4 diffusivity due to the blockage of the intersections by benzene.[23] In the process of the alkylation of benzene using H-ZSM-5 catalyst to produce ethylbenzene, the tardier aromatic molecules prefer to locate at the channel intersections. The blocking of the intersections by the aromatic guests causes a severe reduction in the effective diffusivity of the reactant C_2H_4.[8,9]

The primary objective of this article is to examine the characteristics of the M−S diffusivities $Đ_1$, $Đ_2$, and $Đ_{12}$ applicable to the traffic junction phenomena witnessed in Figure 1. Specifically, we aim to show that for diffusion in the *n*C4(1)/*i*C4(2) mixtures, the M−S diffusivity of the more mobile *n*C4, $Đ_1$, is significantly lower than that of the corresponding unary *n*C4. Furthermore, we shall establish that the reduction in the diffusivity of *n*C4 is not attributable to the usual "correlation" effects. Due to the extremely low values of the diffusivities of *i*C4, the MD simulations of the *n*C4/*i*C4 diffusion to determine the M−S diffusivities are of low accuracy and also computationally expensive. For this reason, we resort to the kinetic Monte Carlo (KMC) simulations using the methodology detailed in earlier publications.[24−31]

2. COMPUTATIONAL METHODS: KMC SIMULATIONS

The KMC simulation methodology employed for the MFI lattice topology is shown schematically in Figure 2. Per unit

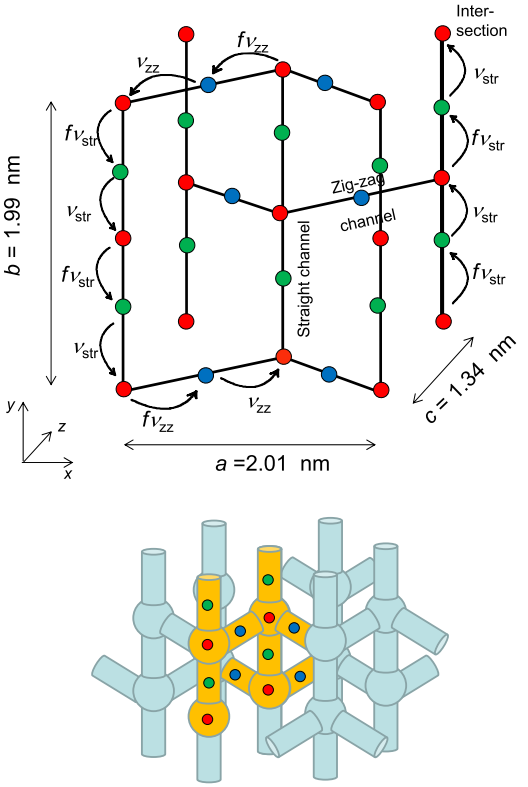

Figure 2. Schematic of the KMC simulation methodology for the MFI topology consisting of the intersecting straight and zigzag channels. The inset indicates a unit cell (highlighted in orange), with 12 adsorption sites.

cell, highlighted in orange in the inset, is made up of 12 adsorption sites, distributed along the straight channels (4, marked green), zigzag channels (4, marked blue), and at the intersections (4, marked red). A total of 2 × 2 × 4 = 16 unit cells were used. In the KMC simulations, we assume that the each site can be occupied by only one molecule at a time. Particles can move from one site to a neighboring site via hops. Let ν_{str} and ν_{zz} denote the jump frequencies along the straight

DOI: 10.1021/acsomega.9b01369
ACS Omega 2019, 4, 10761−10766

and zigzag channels when moving toward the intersections. Based on the MD simulations of the self-diffusivities of guest molecules in x-, y-, and z-directions (see Figure S13),[32] it is concluded that the frequency along the straight channels ν_{str} is greater than that along the zigzag channels ν_{zz} by a factor of about 2. Further details of the KMC simulation methodology are provided in the Supporting Information.

3. RESULTS AND DISCUSSION

We first undertake the KMC simulations of the nC4/iC4 mixture diffusion to match with the experiments of Fernandez et al.[21] in Figure 1b. The preferential location of branched alkanes, such as iC4, at the intersection sites can be modeled by taking the jump frequencies away from the intersection sites to be lower by a factor f than the corresponding frequencies ν_{str} and ν_{zz}.[31] This factor f is determined by the ratio of the Langmuir constants in the dual-site Langmuir fits

$$q = q_{A,sat}\frac{b_A p}{1 + b_A p} + q_{B,sat}\frac{b_B p}{1 + b_B p} \quad (4)$$

for the unary iC4 isotherm at 363 K in Figure 3a; we determine $f = b_B/b_A = 0.001$; calculation details are provided in the Supporting Information. For nC4, there are no perceptible isotherm inflections, and the jump frequencies toward and away from the intersection sites are equal, i.e., $f = 1$. With the chosen values of the jump frequencies ν_{str} and ν_{zz} for nC4 ($\nu_{str} = 4 \times 10^{10}$ s^{-1}; $\nu_{zz} = 2 \times 10^{10}$ s^{-1}; $f = 1$) and iC4 ($\nu_{str} = 4 \times 10^{10}$ s^{-1}; $\nu_{zz} = 2 \times 10^{10}$ s^{-1}; $f = 0.001$), the KMC simulations of the self-diffusivities are shown in Figure 3b; the reduction in the nC4 self-diffusivity by 2 orders of magnitude with increasing iC4 loadings are in line with the experimental data in Figure 1b.

Remarkably, the M−S diffusivity $Đ_1$ for nC4 also shows a lowering of 2 orders of magnitude with increasing proportions of iC4 in the mixture (see Figure 3c). Within the framework of the M−S formulation (eq 1), a reduction in $Đ_1$ does not fall within the purview of the "correlation effects". For the transient uptake of the nC6/2MP mixtures in MFI zeolite crystals, Titze et al.[33] found that the M−S diffusivities of both nC6 and 2MP decrease strongly with increasing 2MP loading, which is analogous to that observed Figure 3c. Indeed, for nC6/2MP separations in fixed beds of MFI zeolite, both intracrystalline diffusion and mixture adsorption in the MFI favor the linear isomer, leading to the highly effective separations in fixed-bed adsorption devices.[18,33,34]

Figure 4a shows KMC simulations for nC4/2MP mixtures in which the chosen jump frequencies of the bulkier 2MP are taken to be a factor 10 lower than those for iC4: ($\nu_{str} = 4 \times 10^9$ s^{-1}; $\nu_{zz} = 2 \times 10^9$ s^{-1}; $f = 0.001$). The reduction of the M−S diffusivity of nC4 is practically the same as that for iC4, even though 2MP is 10 times tardier than iC4; this finding strengthens the hypothesis that the lowering is not caused by correlated hops in the MFI channels. The KMC simulations for the mixtures of propane(C3)/iC4 mixtures, wherein the jump frequencies of C3 are a factor of 2 higher than those for nC4, show that the influence of increased iC4 loading on the M−S diffusivities of the linear alkanes are entirely analogous (see Figure 4b).

To demonstrate that the results in Figures 3 and 4 are distinctly different from the correlation effects, we performed KMC simulations for nC4 in partnership with a "hypothetical" guest species iC4* in which the jump frequencies for iC4* are prescribed as ($\nu_{str} = 4 \times 10^7$ s^{-1}; $\nu_{zz} = 2 \times 10^7$ s^{-1}; $f = 1$), i.e., a factor of 10^3 lower than those for nC4 but without preference to locate at the intersections. Figure 5a compares the M−S diffusivities for the nC4/iC4 and nC4/iC4* mixture diffusion; these show that the M−S diffusivities for the hypothetical

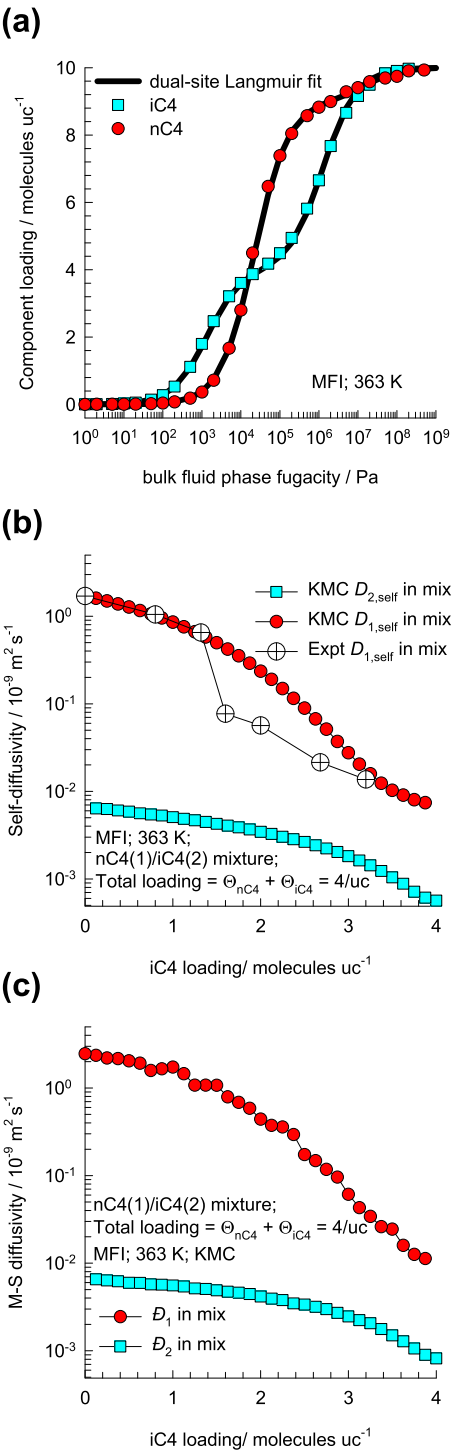

Figure 3. (a) Configurational-bias Monte Carlo simulations of the unary isotherms of nC4 and iC4 at 363 K in MFI zeolite.[21] (b, c) KMC simulations of self- and M−S diffusivities of nC4(1) and iC4(2) for mixture diffusion (total loading is held constant at 4 molecules uc^{-1}) as a function of the iC4 loading. The isotherm fit parameters and further computational details are provided in the Supporting Information.

DOI: 10.1021/acsomega.9b01369
ACS Omega 2019, 4, 10761−10766

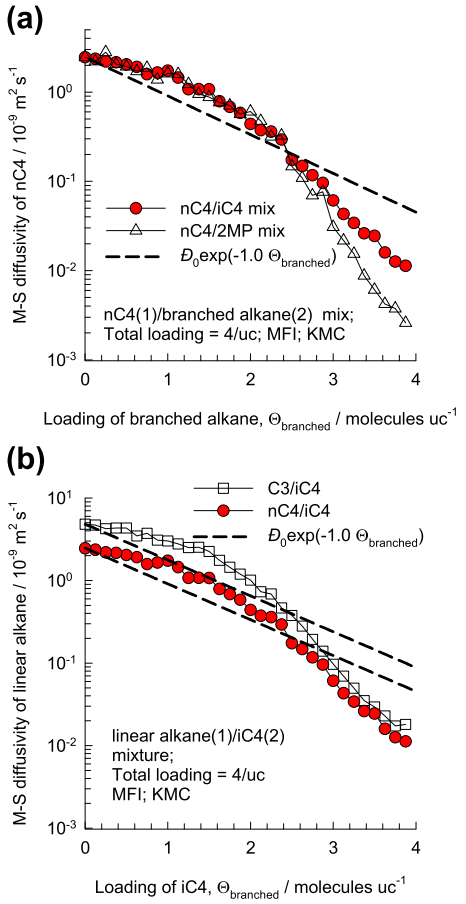

Figure 4. (a) KMC simulation results for M−S diffusivities of *n*C4 in the *n*C4/*i*C4 and *n*C4/2MP mixtures (total loading is held constant at 4 molecules uc^{-1}) as a function of the loading of the branched alkane. (b) KMC simulation results for the M−S diffusivities of linear alkanes in the C3/*i*C4 and *n*C4/*i*C4 mixtures (total loading is held constant at 4 molecules uc^{-1}) as a function of the loading of the branched alkane. Further computational details are provided in the Supporting Information.

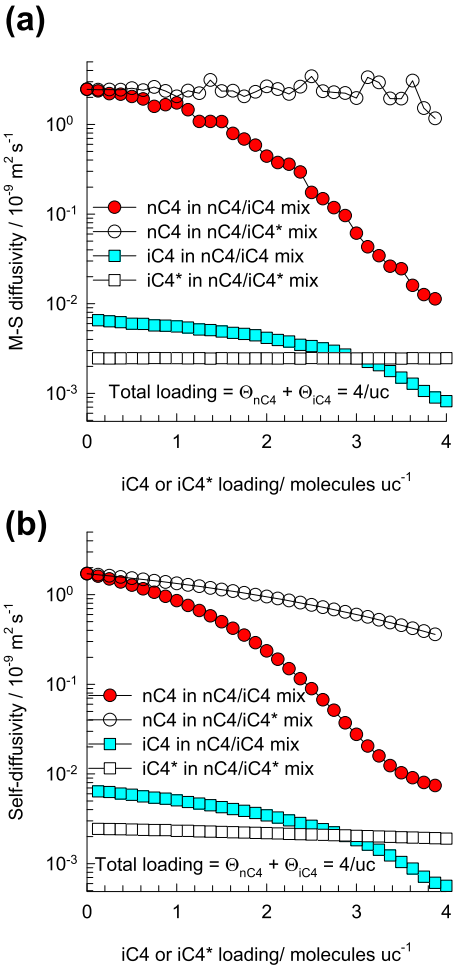

Figure 5. KMC simulation results for (a) M−S diffusivities and (b) self-diffusivities for (a) *n*C4/*i*C4 and *n*C4/*i*C4* mixture diffusion (total loading is held constant at 4 molecules uc^{-1}) as a function of *i*C4 or *i*C4* loading. Further computational details are provided in the Supporting Information.

*n*C4/*i*C4* mixture are independent of *i*C4* loading, as expected for "normal" mixtures without preferential locations of guest molecules. The corresponding values of the self-diffusivities are compared in Figure 5b. The self-diffusivity of *n*C4 in the *n*C4/*i*C4* mixtures is reduced by a factor of about 3, whereas the corresponding reduction for the *n*C4/*i*C4 mixtures is reduced by 2 orders of magnitude. The inescapable conclusion to be drawn from the KMC simulations in Figure 5 is that traffic junction effects do not fall under the category of correlation effects.

To unravel the reasons for the reduction in the M−S diffusivity of *n*C4, with increased *i*C4 loading, we undertook KMC simulations in which certain number of intersection sites in the 2 × 2 × 4 = 16 unit cells are selected and subsequently deleted, along with the connections to the adjoining straight and zigzag channels. The blocking and deletion procedure is illustrated in Figure 6; further elaboration and details are available in the Supporting Information. Evidently, blocking of the intersection sites results in a decrease in the connectivity of the MFI topology. Five different % blocking effects were simulated: 6.25, 12.5, 25, 37.5, and 50%, corresponding to the deletion of 4, 8, 12, 18, and 32 of the total 64 intersection sites in the 2 × 2 × 4 simulation box.

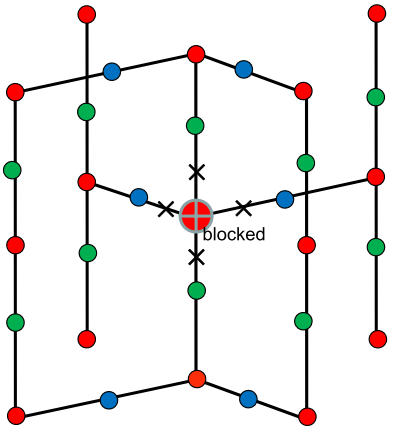

Figure 6. MFI topology in which the intersection site at the center is blocked and the adjoining connections are deleted (indicated by crosses).

Figure 7 presents the KMC simulation results for the influence of the degree of intersection blocking on the M−S diffusivity, $Đ_1$, and degrees of correlation, $Đ_1/Đ_{11}$, for the *n*C4 diffusion in the MFI zeolite. The unary M−S diffusivities are well described by

DOI: 10.1021/acsomega.9b01369
ACS Omega 2019, 4, 10761−10766

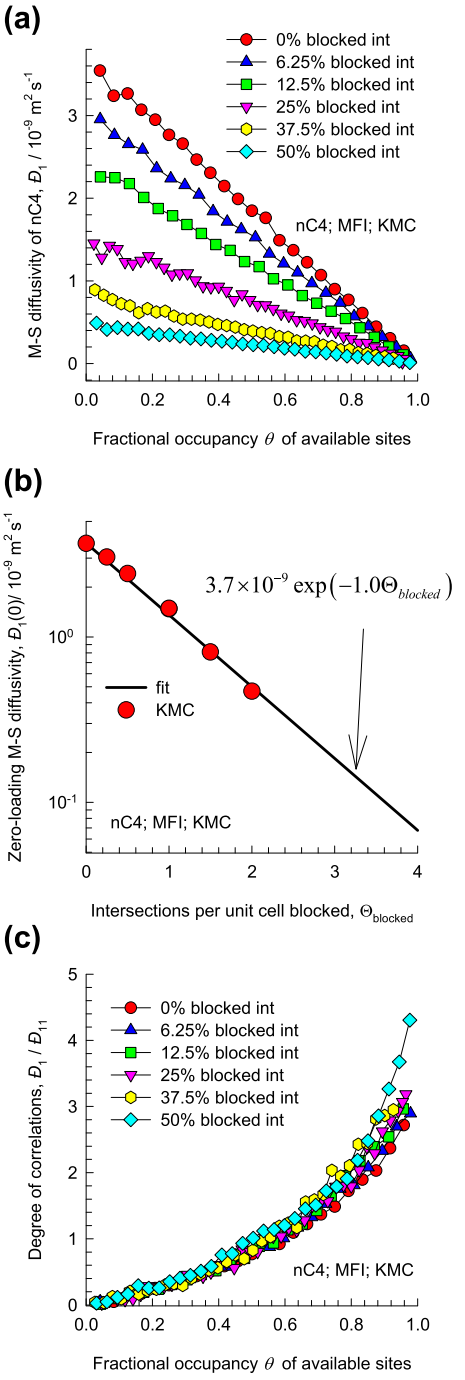

Figure 7. (a, b) KMC simulation results for the influence of the degree of intersection blocking on M−S diffusivity, $Đ_1$, and degrees of correlation, $Đ_1/Đ_{11}$, for the *n*C4 diffusion in the MFI zeolite. The fractional occupancy is the total loading divided by the total number of available adsorption sites after the deletion of the selected number of intersection sites. (c) Zero-loading M−S diffusivity as a function of the number of blocked intersection sites per unit cell.

$$Đ_1 = Đ_1(0)(1 - \theta) \tag{5}$$

where $Đ_1(0)$ is the M−S diffusivity at "zero-loading", and the fractional occupancy θ is the total loading divided by the total number of available adsorption sites after the deletion of the selected number of intersection sites. For the unblocked topology, the zero-loading M−S diffusivity is $Đ_1(0) = 3.7 \times 10^{-9}$ m^2 s^{-1}. The zero-loading M−S diffusivity $Đ_1(0)$ decreases exponentially with the number of blocked intersection sites in one unit cell, $3.7 \times 10^{-9} \exp(-1.0\ \Theta_{blocked})$ (see Figure 7b). The dashed lines in Figure 4a,b compare the exponential decay model with the KMC data for the *n*C4/*i*C4, *n*C4/2MP, and C3/*i*C4 mixtures. Though there are some quantitative differences, the exponential decay model captures the essential characteristics of the reduction in the M−S diffusivity of linear alkanes, suggesting that traffic junction effects are primarily attributable to significant decrease in the connectivity of the MFI topology by blocked intersections.

4. CONCLUSIONS

Kinetic Monte Carlo simulations, in conjunction with the Maxwell−Stefan diffusion formulation, were used to investigate the traffic junction effects that manifest for the mixtures of linear alkane and branched alkanes. The KMC simulations of the *n*C4/*i*C4, *n*C4/2MP, and C3/*i*C4 mixtures at a constant total loading of 4 molecules per unit cell serve to establish that the diffusivity of the linear alkane suffers a decrease of about 2 orders of magnitude when the loading of the branched partner molecule is increased; this is in line with the published experimental data. The reasons for this reduction in the diffusivity of the linear alkane are unequivocally traceable to the loss of connectivity in the MFI topology due to the effective blocking of the intersection sites by ensconced branched molecules. The KMC simulations also establish that traffic junction effects are distinctly different from the correlation effects that manifest for the mixtures in which none of the components exhibits preferential adsorption at the intersection sites.

The results of this study have ramifications for the implementation of the Maxwell−Stefan diffusion model in the design of catalytic reactors, fixed-bed adsorbers, and membrane permeation devices.[8,9,18]

■ ASSOCIATED CONTENT

Supporting Information

The Supporting Information is available free of charge on the ACS Publications website at DOI: 10.1021/acsomega.9b01369.

Provides (a) the structural details for MFI zeolite, (b) Maxwell−Stefan diffusion formulation, (c) kinetic Monte Carlo simulation methodology, including procedures for the calculation of the Maxwell−Stefan diffusivities, (d) KMC simulation data for unary and binary systems (PDF)

■ AUTHOR INFORMATION

Corresponding Author

*E-mail: r.krishna@contact.uva.nl.

ORCID

Rajamani Krishna: 0000-0002-4784-8530

Notes

The authors declare no competing financial interest.

■ ACKNOWLEDGMENTS

The authors express their gratitude to Dr D. Paschek for developing the initial version of the KMC code.

DOI: 10.1021/acsomega.9b01369
ACS Omega 2019, 4, 10761−10766

NOMENCLATURE

Latin Alphabet

$Đ_i$, Maxwell−Stefan diffusivity for molecule−wall interaction, $m^2\ s^{-1}$
$Đ_i(0)$, M−S diffusivity at zero loading, $m^2\ s^{-1}$
$Đ_{12}$, M−S exchange coefficient for binary mixture, $m^2\ s^{-1}$
$D_{i,self}$, self-diffusivity of species i, $m^2\ s^{-1}$
f, ratio of frequencies away and toward intersections, dimensionless
N_i, molecular flux of species i with respect to framework, molecules $m^{-2}\ s^{-1}$
R, gas constant, 8.314 J $mol^{-1}\ K^{-1}$
T, absolute temperature, K
x_i, mole fraction of species i in adsorbed phase, dimensionless

Greek Alphabet

μ_i, molar chemical potential of component i, J mol^{-1}
θ, fractional occupancy, dimensionless
Θ_i, loading of species i, molecules uc^{-1}
ν, jump frequency, s^{-1}
ρ, framework density, uc m^{-3}

Subscripts

1, referring to component 1
2, referring to component 2

REFERENCES

(1) Baerlocher, C.; Meier, W. M.; Olson, D. H. *Atlas of Zeolite Framework Types*, 5th ed.; Elsevier: Amsterdam, 2002.
(2) Degnan, T. F. The Implications of the Fundamentals of Shape Selectivity for the Development of Catalysts for the Petroleum and Petrochemical Industries. *J. Catal.* **2003**, *216*, 32−46.
(3) Marcilly, C. Present status and future trends in catalysis for refining and petrochemicals. *J. Catal.* **2003**, *216*, 47−62.
(4) Corma, A. State of the Art and Future Challenges of Zeolites as Catalysts. *J. Catal.* **2003**, *216*, 298−312.
(5) Čejka, J.; Corma, A.; Zones, S. *Zeolites and Catalysis: Synthesis, Reactions and Applications*; Wiley-VCH: Weinheim, 2010.
(6) Vermeiren, W.; Gilson, J.-P. Impact of Zeolites on the Petroleum and Petrochemical Industry. *Top. Catal.* **2009**, *52*, 1131−1161.
(7) Kulprathipanja, S. *Zeolites in Industrial Separation and Catalysis*; Wiley-VCH: Weinheim, 2010.
(8) Hansen, N.; Krishna, R.; van Baten, J. M.; Bell, A. T.; Keil, F. J. Analysis of Diffusion Limitation in the Alkylation of Benzene over H-ZSM-5 by Combining Quantum Chemical Calculations, Molecular Simulations, and a Continuum Approach. *J. Phys. Chem. C* **2009**, *113*, 235−246.
(9) Hansen, N.; Krishna, R.; van Baten, J. M.; Bell, A. T.; Keil, F. J. Reactor simulation of benzene ethylation and ethane dehydrogenation catalyzed by ZSM-5: A multiscale approach. *Chem. Eng. Sci.* **2010**, *65*, 2472−2480.
(10) Krishna, R.; Baur, R.; Van Baten, J. M. Highlighting Diffusional Coupling Effects in Zeolite Catalyzed Reactions by Combining the Maxwell-Stefan and Langmuir-Hinshelwood Formulations. *React. Chem. Eng.* **2017**, *2*, 324−336.
(11) Krishna, R.; van Baten, J. M. In Silico Screening of Zeolite Membranes for CO_2 Capture. *J. Membr. Sci.* **2010**, *360*, 323−333.
(12) Sandström, L.; Sjöberg, E.; Hedlund, J. Very high flux MFI membrane for CO_2 separation. *J. Membr. Sci.* **2011**, *380*, 232−240.
(13) Krishna, R. Thermodynamic Insights into the Characteristics of Unary and Mixture Permeances in Microporous Membranes. *ACS Omega* **2019**, *4*, 9512−9521.
(14) Krishna, R.; van Baten, J. M. Investigating the Influence of Diffusional Coupling on Mixture Permeation across Porous Membranes. *J. Membr. Sci.* **2013**, *430*, 113−128.
(15) Krishna, R. Using the Maxwell-Stefan formulation for Highlighting the Influence of Interspecies (1-2) Friction on Binary Mixture Permeation across Microporous and Polymeric Membranes. *J. Membr. Sci.* **2017**, *540*, 261−276.
(16) Krishna, R. Describing the Diffusion of Guest Molecules inside Porous Structures. *J. Phys. Chem. C* **2009**, *113*, 19756−19781.
(17) Krishna, R. Diffusion in Porous Crystalline Materials. *Chem. Soc. Rev.* **2012**, *41*, 3099−3118.
(18) Krishna, R. The Maxwell-Stefan Description of Mixture Diffusion in Nanoporous Crystalline Materials. *Microporous Mesoporous Mater.* **2014**, *185*, 30−50.
(19) Krishna, R. Occupancy Dependency of Maxwell−Stefan Diffusivities in Ordered Crystalline Microporous Materials. *ACS Omega* **2018**, *3*, 15743−15753.
(20) Krishna, R.; van Baten, J. M. Maxwell-Stefan modeling of slowing-down effects in mixed gas permeation across porous membranes. *J. Membr. Sci.* **2011**, *383*, 289−300.
(21) Fernandez, M.; Kärger, J.; Freude, D.; Pampel, A.; van Baten, J. M.; Krishna, R. Mixture Diffusion in Zeolites Studied by MAS PFG NMR and Molecular Simulation. *Microporous Mesoporous Mater.* **2007**, *105*, 124−131.
(22) Schuring, D.; Koriabkina, A. O.; de Jong, A. M.; Smit, B.; van Santen, R. A. Adsorption and Diffusion of n-hexane/2-methylpentane Mixtures in Zeolite Silicalite: Experiments and Modeling. *J. Phys. Chem. B* **2001**, *105*, 7690−7698.
(23) Förste, C.; Germanus, A.; Kärger, J.; Pfeifer, H.; Caro, J.; Pilz, W.; Zikánová, A. Molecular Mobility of Methane Adsorbed in ZSM-5 Containing Co-adsorbed Benzene, and the Location of Benzene Molecules. *J. Chem. Soc., Faraday Trans. 1* **1987**, *83*, 2301−2309.
(24) Paschek, D.; Krishna, R. Monte Carlo simulations of self- and transport-diffusivities of 2-methylhexane in silicalite. *Phys. Chem. Chem. Phys.* **2000**, *2*, 2389−2394.
(25) Paschek, D.; Krishna, R. Diffusion of binary mixtures in zeolites: Kinetic Monte Carlo versus molecular dynamics simulations. *Langmuir* **2001**, *17*, 247−254.
(26) Paschek, D.; Krishna, R. Monte Carlo simulations of sorption and diffusion of isobutane in silicalite. *Chem. Phys. Lett.* **2001**, *342*, 148−154.
(27) Krishna, R.; van Baten, J. M.; Dubbeldam, D. On the Inflection in the Concentration Dependence of the Maxwell-Stefan diffusivity of CF_4 in MFI zeolite. *J. Phys. Chem. B* **2004**, *108*, 14820−14822.
(28) Krishna, R.; van Baten, J. M. Kinetic Monte Carlo simulations of the loading dependence of diffusion in zeolites. *Chem. Eng. Technol.* **2005**, *28*, 160−167.
(29) Krishna, R.; Paschek, D. Verification of the Maxwell-Stefan theory for tracer diffusion in zeolites. *Chem. Eng. J.* **2002**, *85*, 7−15.
(30) Krishna, R.; Paschek, D.; Baur, R. Modelling the occupancy dependence of diffusivities in zeolites. *Microporous Mesoporous Mater.* **2004**, *76*, 233−246.
(31) Chmelik, C.; Heinke, L.; Kärger, J.; Shah, D. B.; Schmidt, W.; van Baten, J. M.; Krishna, R. Inflection in the Loading Dependence of the Maxwell-Stefan Diffusivity of Iso-butane in MFI Zeolite. *Chem. Phys. Lett.* **2008**, *459*, 141−145.
(32) Krishna, R.; van Baten, J. M. Diffusion of Hydrocarbon Mixtures in MFI Zeolite: Influence of Intersection Blocking. *Chem. Eng. J.* **2008**, *140*, 614−620.
(33) Titze, T.; Chmelik, C.; Kärger, J.; van Baten, J. M.; Krishna, R. Uncommon Synergy Between Adsorption and Diffusion of Hexane Isomer Mixtures in MFI Zeolite Induced by Configurational Entropy Effects. *J. Phys. Chem. C* **2014**, *118*, 2660−2665.
(34) Krishna, R. Methodologies for Evaluation of Metal-Organic Frameworks in Separation Applications. *RSC Adv.* **2015**, *5*, 52269−52295.

DOI: 10.1021/acsomega.9b01369
ACS Omega 2019, 4, 10761−10766

Elucidating Traffic Junction Effects in MFI Zeolite using Kinetic Monte Carlo Simulations

Rajamani Krishna* and Jasper M. van Baten

Van 't Hoff Institute for Molecular Sciences
University of Amsterdam
Science Park 904
1098 XH Amsterdam, The Netherlands
email: r.krishna@contact.uva.nl

Table of Contents

1 Preamble

The Supporting Information accompanying our article *Elucidating Traffic Junction Effects in MFI Zeolite using Kinetic Monte Carlo Simulations* provides (a) structural details for MFI zeolite, (b) Maxwell-Stefan diffusion formulation, (c) Kinetic Monte Carlo simulation methodology, including procedures for calculation of the Maxwell-Stefan diffusivities, (d) KMC simulation data for unary and binary systems.

For ease of reading, the Supporting Information is written as a stand-alone document; as a consequence, there is some overlap of material with the main manuscript.

2 Structural details of MFI zeolite

MFI zeolite (also called ZSM-5) has a topology consisting of a set of intersecting straight and zig-zag (or sinusoidal) channels of approximately 5.5 Å size. The pore landscapes and structural details are provided in Figure S1, and Figure S2. The crystallographic data are available on the zeolite atlas website of the International Zeolite Association (IZA).[1] The data on surface area, pore volume, and effective pore diameters are taken from earlier work,[2] and summarized in Figure S1, and Figure S2.

2.1 List of Figures for Structural details of MFI zeolite

	MFI
a /Å	20.022
b /Å	19.899
c /Å	13.383
Cell volume / Å^3	5332.025
conversion factor for [molec/uc] to [mol per kg Framework]	0.1734
conversion factor for [molec/uc] to [kmol/m^3]	1.0477
ρ [kg/m3]	1796.386
MW unit cell [g/mol(framework)]	5768.141
ϕ, fractional pore volume	0.297
open space / Å^3/uc	1584.9
Pore volume / cm^3/g	0.165
Surface area /m^2/g	487.0
DeLaunay diameter /Å	5.16

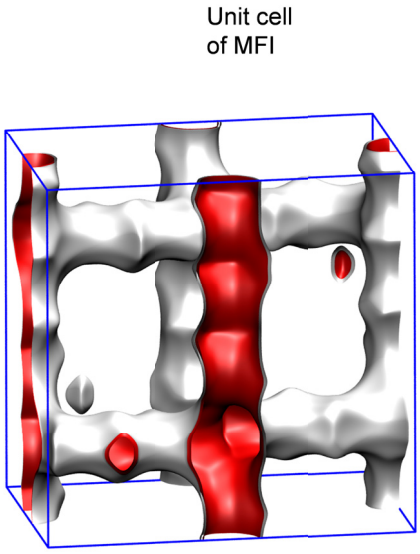

Structural information from: C. Baerlocher, L.B. McCusker,
Database of Zeolite Structures, International Zeolite Association,
http://www.iza-structure.org/databases/

Figure S1. Structural details and pore landscape for MFI zeolite.

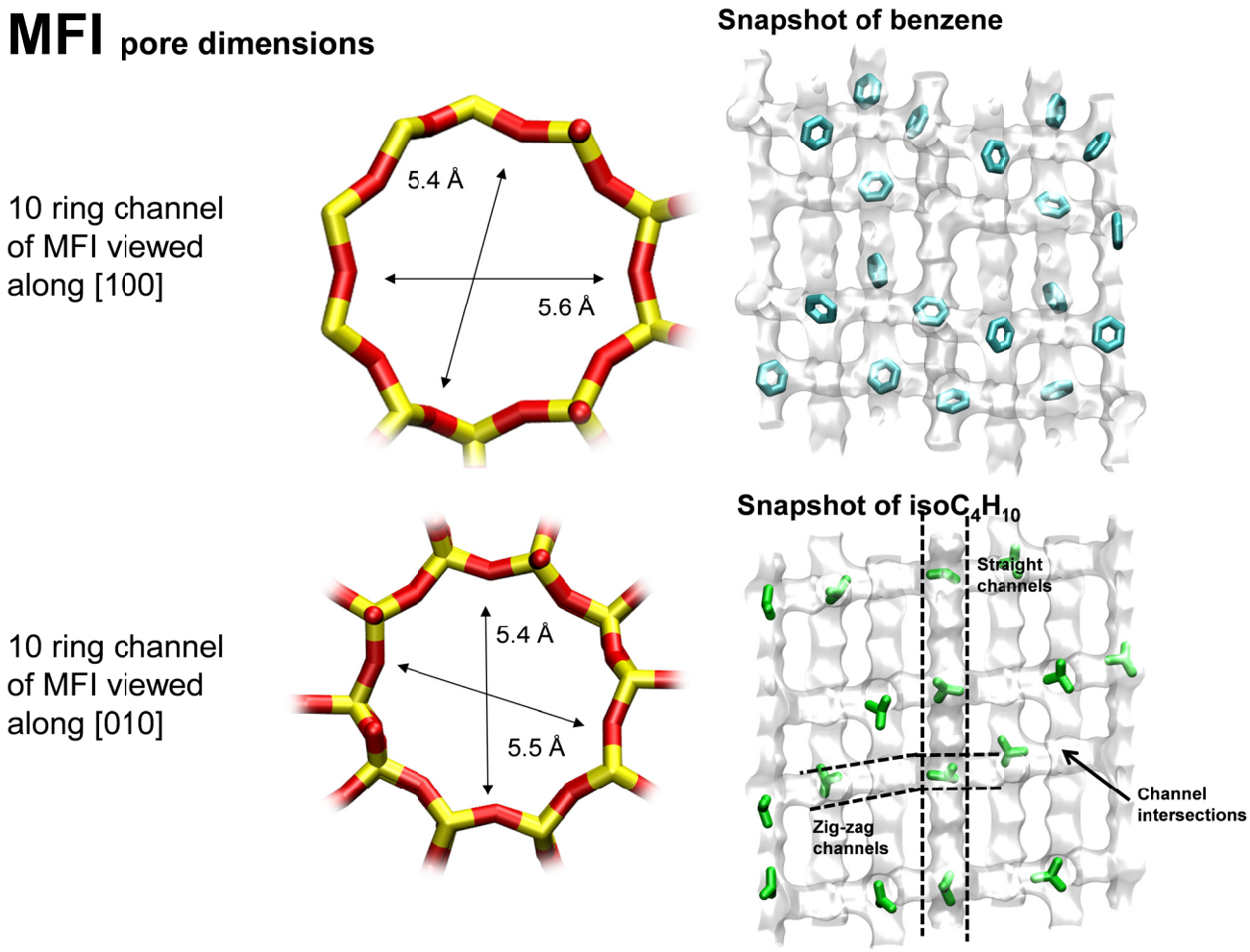

Figure S2. Structural details and pore landscape for MFI zeolite.

3 Experimental data highlighting traffic junction effects

A set of five different experimental data sets, along with computational snapshots, are considered in Figure S3, Figure S4, Figure S5, Figure S6, Figure S7, and Figure S8.

In the PFG NMR investigation of Fernandez et al.[3] the self-diffusivity in MFI of n-butane (nC4), in mixtures with iso-butane (iC4), was found to decrease by about two orders of magnitude as the loading of iC4 is increased from $\Theta_{iC4} = 0$ to 2 molecules per unit cell; see Figure S3(b). The reason for this strong decline can be understood on the basis of the preferential location of iC4 at the channel intersections of MFI. For $\Theta_{iC4} = 2$, half the total number of intersections are occupied by iC4, that has a diffusivity which is about three orders of magnitude lower than that of nC4. Since the occupancy of the intersections is distributed randomly, each of the straight channels has an iC4 molecule ensconced somewhere along the channels; this is evident from the snapshot in Figure S3(a). This is tantamount to blockage and leads to severe reduction in the molecular traffic of the intrinsically more mobile nC4.

Figure S4(a,b,c,d) presents the IRM (Infra-Red Microscopy) experimental data of Chmelik et al.[4] on transient counter-uptake of nC4/iC4 mixtures in MFI zeolite crystals at 298 K. In these experiments, the initial iC4 equilibrated loadings (in units of molecules per unit cell (uc)) in the crystals are 4 uc^{-1}, 2.9 uc^{-1}, 2.2 uc^{-1}, and 1.5 uc^{-1}. The transient uptakes of nC4 are clearly strongly influenced by the initial iC4 loadings, as is evident in the comparison of the nC4 uptakes in Figure S4(e). Figure S4(f) plots the effective diffusivity of nC4 in the coffin-shaped crystals (with dimensions are $160\times25.5\times25.5$ μm^3), as a function of the initial loading of iC4 within the crystals. The values of the fitted nC4 diffusivities can be adequately expressed as the exponential decay with $\Theta_{blocked}$, the initial iC4 loadings in molecules uc^{-1}: $140\times10^{-13}\exp\left(-1.0\Theta_{blocked}\right)$ m^2 s^{-1}. The theoretical justification for this exponential decay function is provided in a later section using Kinetic Monte Carlo (KMC) simulations.

Figure S5 present IRM experimental data of Chmelik on transient co-current adsorption/desorption of nC4/iC4 mixtures in MFI zeolite crystals at 298 K. The co-current uptakes are for (a, d) adsorption

cycles, and (b, e) desorption cycles. The loading trajectories in the adsorption/desorption cycles are plotted in (c, f). Traffic junction effects cause the adsorption/desorption cycles to follow asymmetric trajectories in composition space; see Figure S5(c,f).

PFG NMR studies of Förste et al.[5] found that the self-diffusivity of CH_4 in MFI is significantly reduced as the loading of the co-adsorbed benzene increases; see Figure S6(b). The explanation is again to be found in the hindering of CH_4 diffusion due to blocking of the intersections by benzene.[5]

For analogous reasons, the branched alkanes 2-methylpentane (2MP), causes the reduction in the self-diffusivity of the n-hexane (nC6) in nC6/ 2MP mixtures;[6, 7] see Figure S7.

Titze et al.[8] report the Maxwell-Stefan diffusivity values, $Đ_1/r_c^2$, and $Đ_2/r_c^2$ that are fitted to match experimental data on four sets of experiments for uptake of nC6/2MP mixtures in MFI zeolite crystals; see Figure S8. The diffusivities of both nC6 and 2MP decrease strongly with increased 2MP loading, precisely analogous to that observed by Schuring et al.[6] Clearly, intersection blocking effects are also in play here. We also note a further characteristic for this mixture of more-mobile-more-strongly-adsorbed-nC6 and tardier-less-strongly-adsorbed-2MP. There is uncommon synergy because both adsorption and diffusion favor the linear isomer.[8]

3.1 List of Figures for Experimental data highlighting traffic junction effects

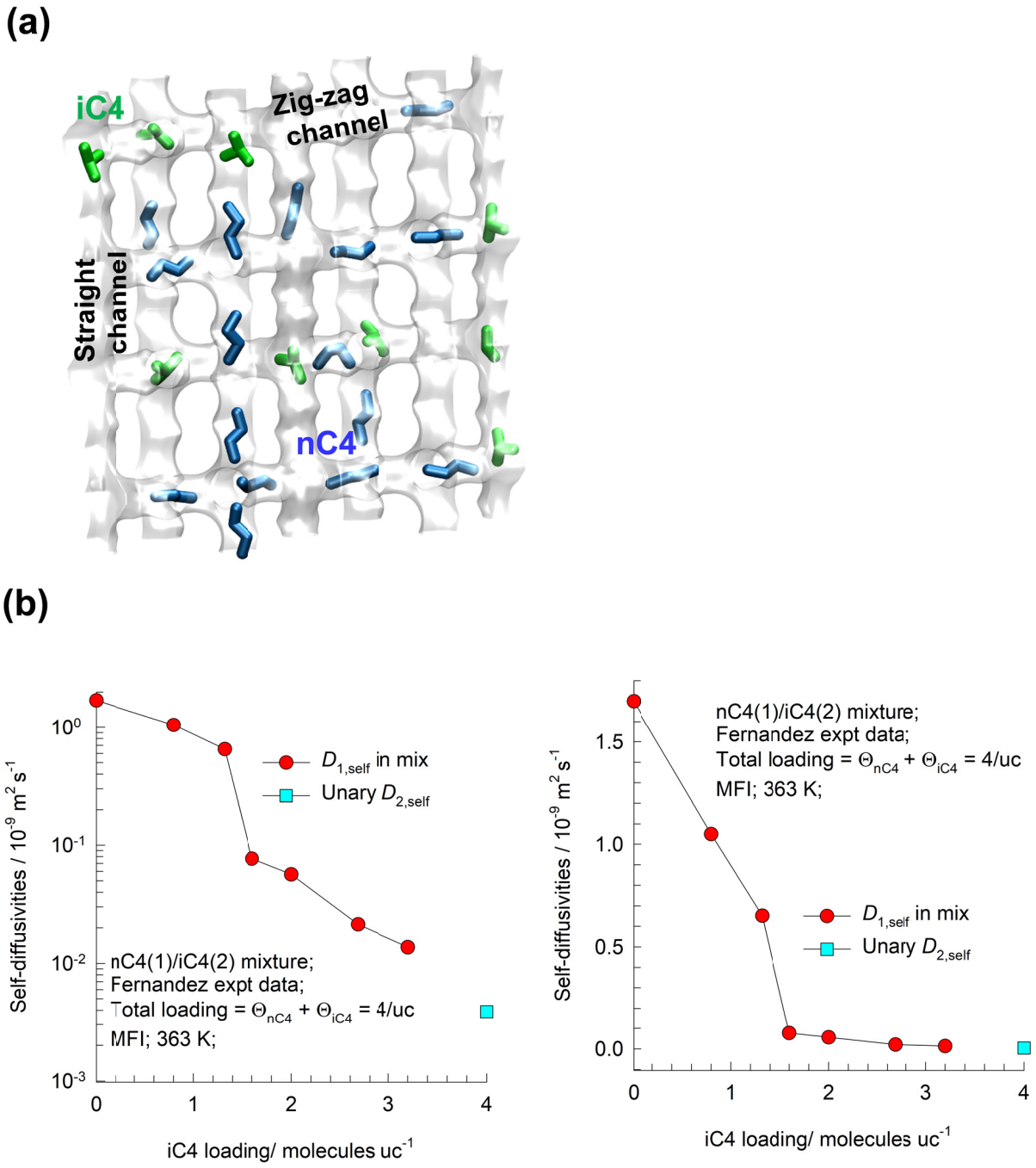

Figure S3. (a) Snapshots showing the location of molecules of nC4/iC4 mixtures in MFI zeolite. (b) PFG NMR experimental data[3] on self-diffusion coefficients of nC4 in nC4/iC4 mixtures in MFI as a function of the loading of iC4.

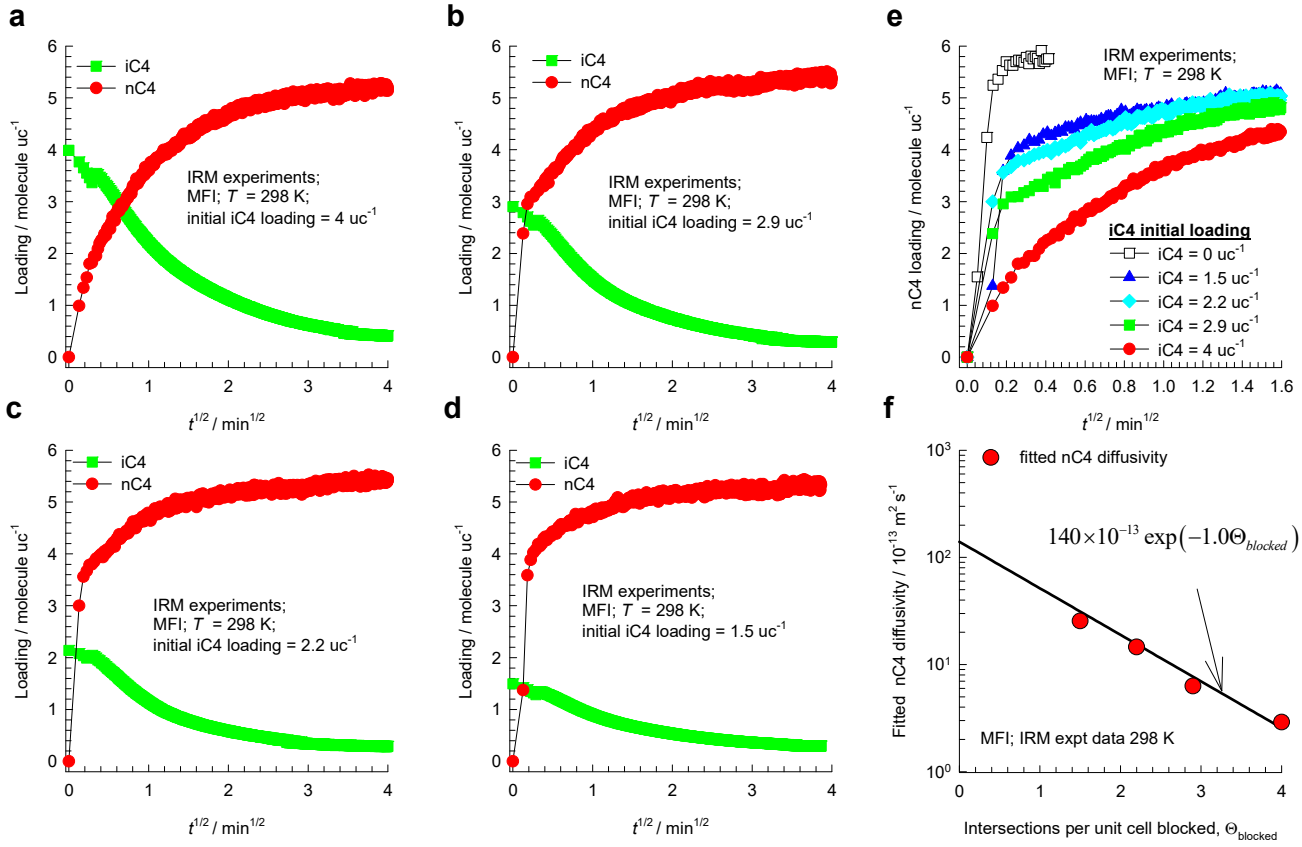

Figure S4. (a, b, c, d) IRM experimental data of Chmelik et al.[4] on transient counter-uptake of nC4/iC4 mixtures in MFI zeolite crystals at 298 K. In these experiments, the initial iC4 equilibrated loadings (in units of molecules per unit cell (uc)) in the crystals are (a) 4 uc^{-1}, (b) 2.9 uc^{-1}, (c) 2.2 uc^{-1}, and (d) 1.5 uc^{-1}. (e) Comparison of transient nC4 uptakes in crystals with different initial iC4 loadings. The experimental IRM data are re-plotted using the data in Figures 3 and 4 of Chmelik et al.[4] (f) Fitted nC4 diffusivity values plotted as a function of the initial iC4 loading in the crystals. The coffin-shaped crystal dimensions are 160×25.5×25.5 μm^3.

Experimental data highlighting traffic junction effects

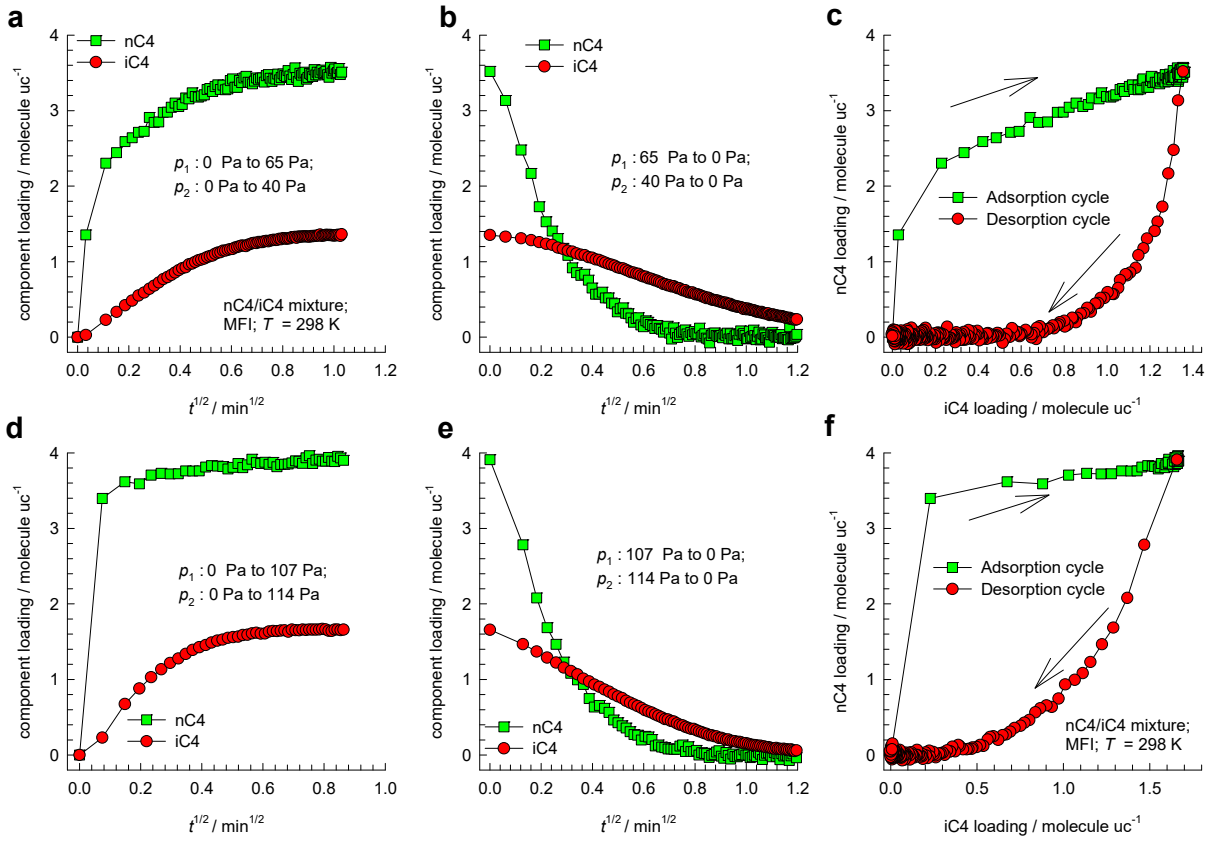

Figure S5. IRM experimental data of Chmelik on transient co-current uptakes of nC4/iC4 mixtures in MFI zeolite crystals at 298 K. The co-current uptakes are for (a, d) adsorption cycles, and (b, e) desorption cycles. The loading trajectories in the adsorption/desorption cycles are plotted in (c, f).

Experimental data highlighting traffic junction effects

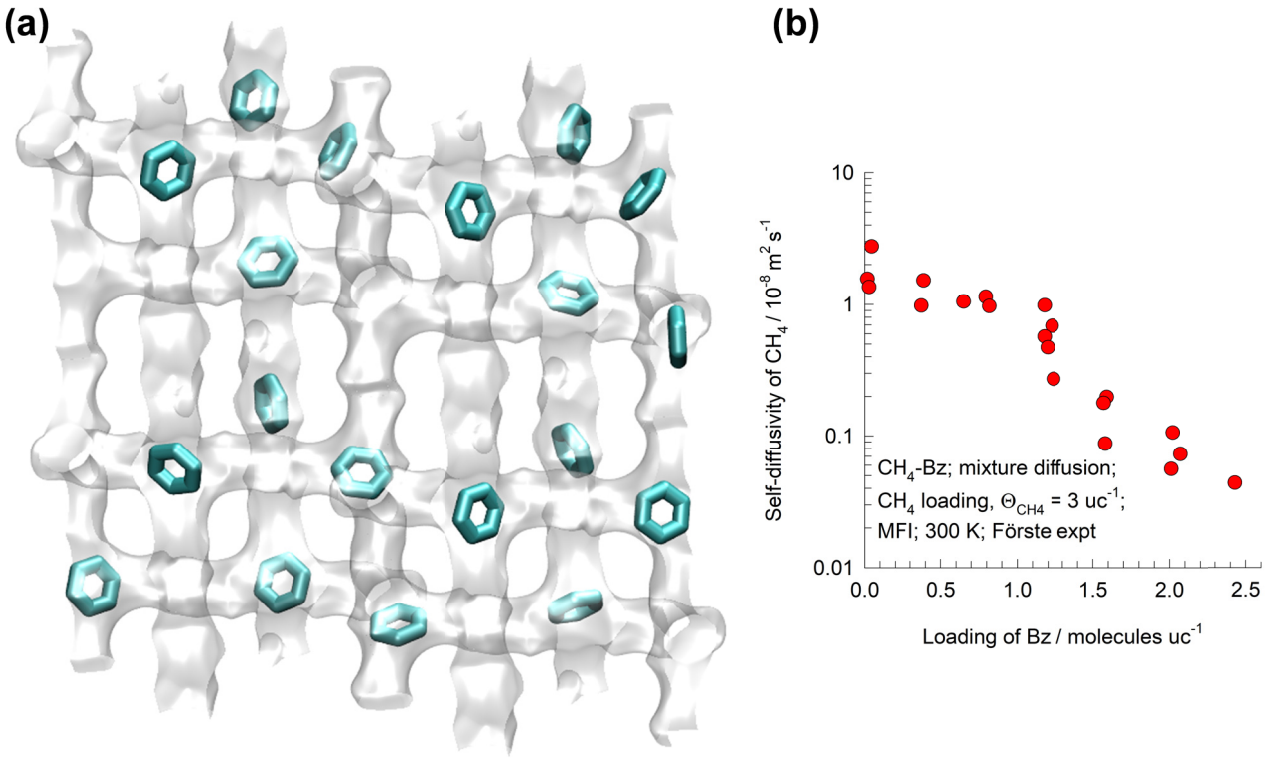

Figure S6. (a) Snapshots showing the location of benzene molecules in MFI zeolite. (b) PFG NMR studies of Förste et al.[5] for the self-diffusivity of CH_4 in MFI as function of the loading of the co-adsorbed benzene in MFI zeolite.

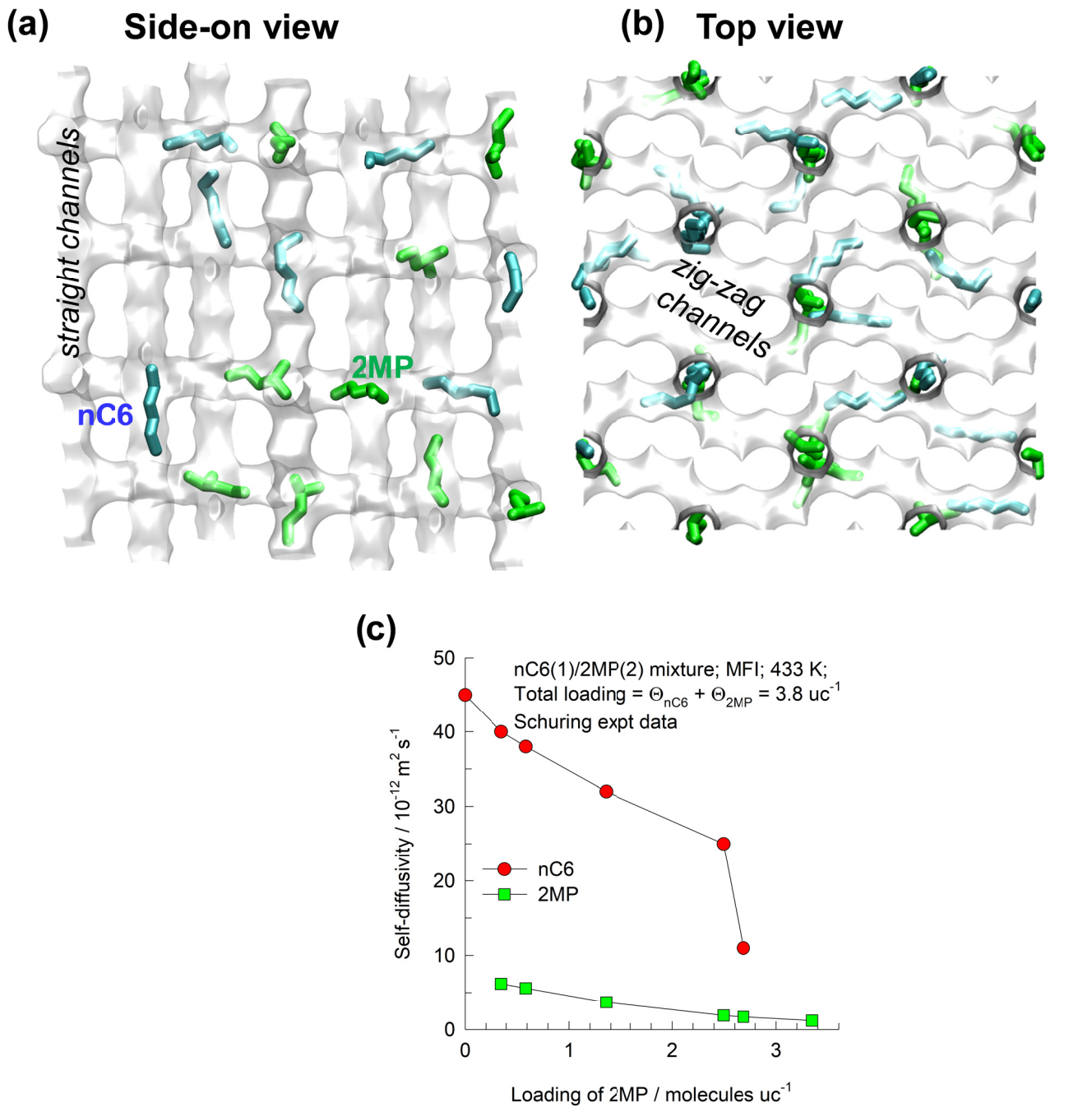

Figure S7. (a, b) Snapshots showing the location of molecules of nC6/2MP mixtures in MFI zeolite. (c) Experimental data[6] on self-diffusivities of nC6 and 2-methylpentane (2MP) as a function of loading of 2MP in MFI zeolite.

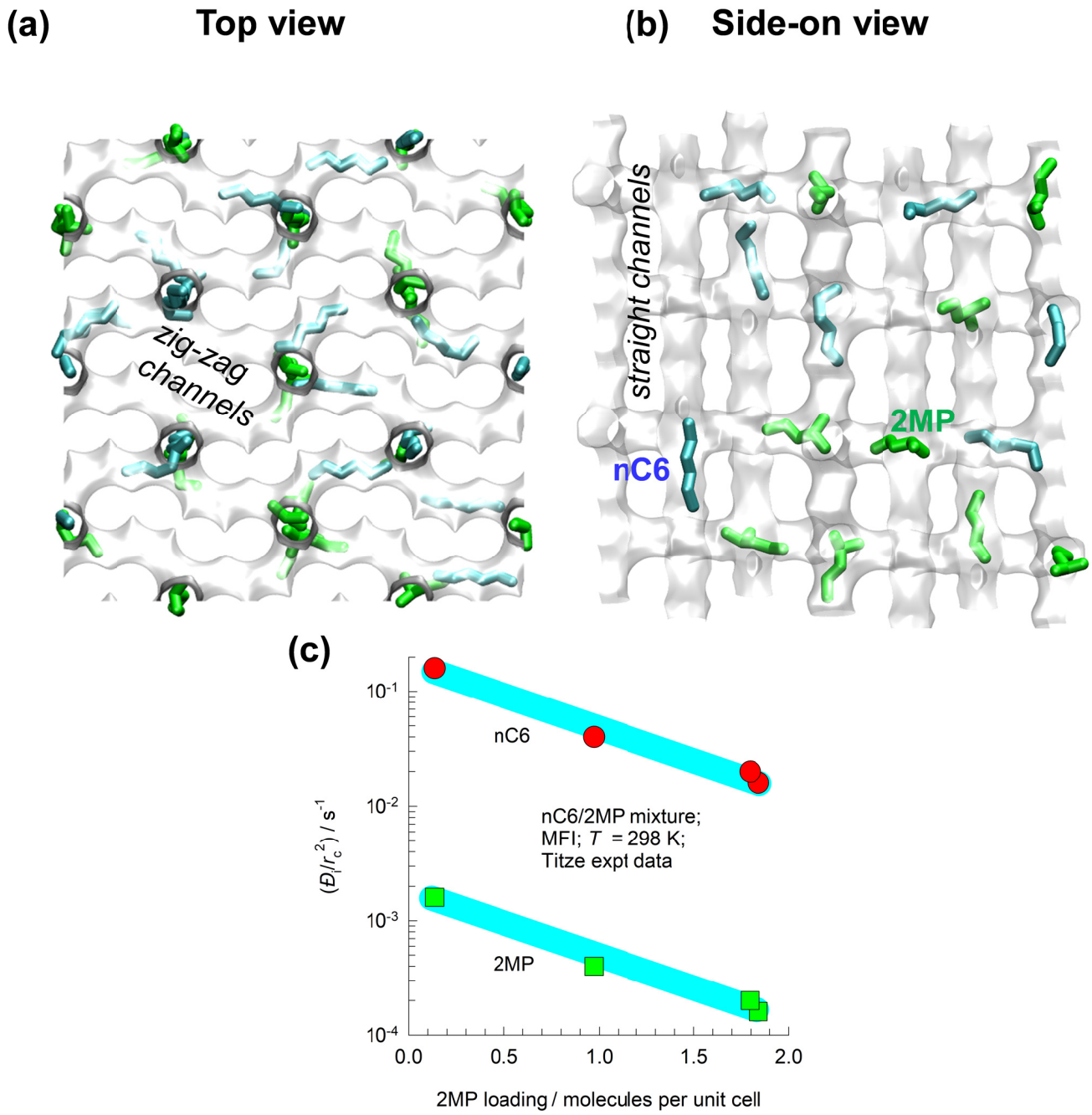

Figure S8. (a, b) Snapshots showing the location of molecules of nC6/2MP mixtures in MFI zeolite. (c) Values of the fitted Maxwell-Stefan diffusivities, $Đ_1/r_c^2$, and $Đ_2/r_c^2$ for nC6 (1) and 2MP (2) chosen to match the four sets of experimental nC6(1)/2MP(2) uptake data of Titze et al.,[8] plotted as a function of the 2MP loading. Here $Đ$ is the Maxwell-Stefan diffusivity, and r_c is the radius of the MFI crystals used in the experimental measurements.

4 The Maxwell-Stefan formulation for diffusion in micropores

4.1 Diffusion in *n*-component mixtures

Within micro-porous crystalline materials, such as zeolites, metal-organic frameworks (MOFs), and zeolitic imidazolate frameworks (ZIFs), the guest molecules exist in the adsorbed phase. The Maxwell-Stefan (M-S) equations for *n*-component diffusion in porous materials is applied in the following manner[2, 9-15]

$$-\rho \frac{q_i}{RT}\frac{d\mu_i}{dz} = \sum_{\substack{j=1 \\ j\neq i}}^{n} \frac{x_j N_i - x_i N_j}{Đ_{ij}} + \frac{N_i}{Đ_i}; \quad i = 1,2,..n \tag{S1}$$

where ρ is the framework density with units of kg m^{-3}, and the fluxes N_i are the number of moles of species *i* transported per m^2 of crystalline material per second. The mole fractions of the components in the adsorbed phase, $x_i = q_i / q_t$ where q_i is the molar loading of adsorbate, and q_t is the *total* mixture loading $q_t = \sum_{i=1}^{n} q_i$. For MFI zeolite it is often convenient to express the loadings in the units of molecules per uc (uc = unit cell); we write

$$-\rho \frac{\Theta_i}{RT}\frac{d\mu_i}{dz} = \sum_{\substack{j=1 \\ j\neq i}}^{n} \frac{x_j N_i - x_i N_j}{Đ_{ij}} + \frac{N_i}{Đ_i}; \qquad i = 1,2,..n \tag{S2}$$

In Equation (S2), the Θ_i are the component loadings expressed in molecules per uc (uc = unit cell), the framework density has the units uc m^{-3}, and the fluxes N_i have the units molecules m^{-2} s^{-1}.

The Maxwell-Stefan diffusion formulation (S1) is consistent with the theory of irreversible thermodynamics. The Onsager Reciprocal Relations imply that the M-S pair diffusivities are symmetric

$$Đ_{ij} = Đ_{ji} \tag{S3}$$

An important, persuasive, argument for the use of the M-S formulation for mixture diffusion is that the M-S diffusivity $Đ_i$ in mixtures can be estimated using information on the loading dependence of the

corresponding unary diffusivity values. Put another way, the M-S diffusivity $Đ_i$ can be estimated from experimental data on *unary* diffusion in the porous material.

The M-S diffusivity $Đ_{ij}$ has the units m^2 s^{-1} and the physical significance of an *inverse* drag coefficient. At the molecular level, the $Đ_{ij}$ reflect how the facility for transport of species *i correlates* with that of species *j*; they are also termed *exchange coefficients*.

4.2 Thermodynamic correction factors

At thermodynamic equilibrium, the chemical potential of component *i* in the bulk fluid mixture equals the chemical potential of that component in the adsorbed phase. For the bulk fluid phase mixture we have

$$\frac{1}{RT}\frac{d\mu_i}{dz} = \frac{d\ln f_i}{dz} = \frac{1}{f_i}\frac{df_i}{dz}; \qquad i = 1,2,..n \tag{S4}$$

The chemical potential gradients $d\mu_i/dz$ can be related to the gradients of the molar loadings, q_i, by defining thermodynamic correction factors Γ_{ij}

$$\frac{q_i}{RT}\frac{d\mu_i}{dz} = \sum_{j=1}^{n}\Gamma_{ij}\frac{dq_j}{dz}; \quad \frac{c_i}{RT}\frac{d\mu_i}{dz} = \sum_{j=1}^{n}\Gamma_{ij}\frac{dc_j}{dz}; \qquad \Gamma_{ij} = \frac{q_i}{f_i}\frac{\partial f_i}{\partial q_j} = \frac{c_i}{p_i}\frac{\partial f_i}{\partial c_j}; \qquad i,j = 1,....n \tag{S5}$$

The thermodynamic correction factors Γ_{ij} can be calculated by differentiation of the model describing mixture adsorption equilibrium. Generally speaking, the Ideal Adsorbed Solution Theory (IAST) of Myers and Prausnitz[16] is the preferred method for estimation of mixture adsorption equilibrium. In the special case in which the unary isotherms for every component is described by the 1-site Langmuir model with equal saturation capacities, the mixed-gas Langmuir model

$$\frac{q_i}{q_{sat}} = \theta_i = \frac{b_i f_i}{1+\sum_{i=1}^{n} b_i f_i}; \quad i = 1,2,...n \tag{S6}$$

is derivable from the IAST. Analytic differentiation of equation (S6) yields

$$\Gamma_{ij} = \delta_{ij} + \left(\frac{\theta_i}{\theta_V} \right); \qquad i, j = 1, 2 \ldots n \tag{S7}$$

where the fractional vacancy θ_V is defined as

$$\theta_V = 1 - \theta_t = 1 - \sum_{i=1}^{n} \theta_i \tag{S8}$$

The elements of the matrix of thermodynamic factors Γ_{ij} can be calculated explicitly from information on the component loadings q_i in the adsorbed phase; this is the persuasive advantage of the use of the mixed-gas Langmuir model. By contrast, the IAST does not allow the calculation of Γ_{ij} explicitly from knowledge on the component loadings q_i in the adsorbed phase; a numerical procedure is required.

4.3 Explicit expression for the fluxes as function of loading gradients

By defining an n-dimensional square matrix $[B]$ with elements

$$B_{ii} = \frac{1}{Đ_i} + \sum_{\substack{j=1 \\ j \neq i}}^{n} \frac{x_j}{Đ_{ij}}; \qquad B_{ij} = -\frac{x_i}{Đ_{ij}}; \quad i, j = 1,2 \ldots . n \tag{S9}$$

we can recast equation (S1) into the following form

$$-\rho \frac{q_i}{RT} \nabla \mu_i = \sum_{j=1}^{n} B_{ij} N_j; \qquad i = 1, 2, .. n \tag{S10}$$

Equation (S10) can be re-written in n-dimensional matrix notation as

$$(N) = -\rho \left[B \right]^{-1} \left[\Gamma \right] \frac{d(q)}{dz} = -\rho \left[\Lambda \right] \left[\Gamma \right] \frac{d(q)}{dz} \tag{S11}$$

We denote the inverse of $[B]$ as $\left[\Lambda \right]$:

$$\left[\Lambda \right] \equiv [B]^{-1} \tag{S12}$$

The elements of $\left[\Lambda \right]$ cannot be determined from experimental measurements. However, Λ_{ij} are directly accessible from Molecular Dynamics (MD) or Kinetic Monte Carlo (KMC) simulations by monitoring the individual molecular displacements

$$\Lambda_{ij} = \frac{1}{2}\lim_{\Delta t\to\infty}\frac{1}{n_j}\frac{1}{\Delta t}\left\langle\left(\sum_{l=1}^{n_i}\left(\mathbf{r}_{l,i}(t+\Delta t)-\mathbf{r}_{l,i}(t)\right)\right)\bullet\left(\sum_{k=1}^{n_j}\left(\mathbf{r}_{k,j}(t+\Delta t)-\mathbf{r}_{k,j}(t)\right)\right)\right\rangle \tag{S13}$$

In this expression n_i and n_j represent the number of molecules of species *i* and *j* respectively, and $\mathbf{r}_{l,i}(t)$ is the position of molecule *l* of species *i* at any time *t*.

Compliance with the Onsager Reciprocal Relations demands

$$n_j\Lambda_{ij} = n_i\Lambda_{ji};\quad i,j = 1,2,....n \tag{S14}$$

4.4 Diffusivities in unary systems

For unary diffusion, equation (S1) simplifies to yield

$$-\rho\frac{q_i}{RT}\frac{d\mu_i}{dz} = \frac{N_i}{Đ_i} \tag{S15}$$

The pure component $Đ_i$ is obtained from MD or KMC simulations of molecular displacements using the formula in each of the coordinate direction

$$Đ_i = \frac{1}{2}\lim_{\Delta t\to\infty}\frac{1}{n_i}\frac{1}{\Delta t}\left\langle\left(\sum_{l=1}^{n_i}\left(\mathbf{r}_{l,i}(t+\Delta t)-\mathbf{r}_{l,i}(t)\right)\right)^2\right\rangle \tag{S16}$$

In this expression n_i represents the number of molecules of species *i*, and $\mathbf{r}_{l,i}(t)$ is the position of molecule *l* of species *i* at any time *t*.

The self-exchange diffusivity, $Đ_{ii}$, is defined by applying the M-S equations to a binary mixture, that consists of identical species, tagged and un-tagged and assuming, furthermore, that we have equimolar diffusion $N_1 + N_2 = 0$. In this special case, the following relation between the self-diffusivity, $D_{i,self}$, and the M-S diffusivity, $Đ_i$, for *unary* diffusion [15]

$$-\rho\frac{q_1}{RT}\frac{d\mu_1}{dz} = \frac{(x_1+x_2)N_1}{Đ_{11}} + \frac{N_1}{Đ_1} = \left(\frac{1}{Đ_{11}}+\frac{1}{Đ_1}\right)N_1 \tag{S17}$$

Equation (S17) defines the self-diffusivity within a pore for this special situation describing "tracer" diffusion

$$-\rho\frac{q_i}{RT}\frac{d\mu_i}{dz}=\frac{N_i}{D_{i.self}} \tag{S18}$$

and so we derive the expression

$$\frac{1}{D_{i,self}}=\frac{1}{Đ_i}+\frac{1}{Đ_{ii}} \tag{S19}$$

The self-diffusivities $D_{\mathrm{i,self}}$ are computed from MD simulations by analyzing the mean square displacement of each species i for each coordinate direction

$$D_{i,self}=\frac{1}{2n_i}\lim_{\Delta t\to\infty}\frac{1}{\Delta t}\left\langle\left(\sum_{l=1}^{n_i}\left(\mathbf{r}_{l,i}(t+\Delta t)-\mathbf{r}_{l,i}(t)\right)^2\right)\right\rangle \tag{S20}$$

Equation (S19) may used to determine the self-exchange diffusivities $Đ_{\mathrm{ii}}$ from MD simulated $D_{\mathrm{i,self}}$ and $Đ_{\mathrm{i}}$ for unary diffusion. The self-exchange diffusivity, $Đ_{\mathrm{ii}}$, quantifies the extent of correlations for unary diffusion. The $Đ_{\mathrm{i}}$, reflecting *collective* motion of molecules (cf. equation (S16)) is free from such correlation effects; it is for this reason that the $Đ_{\mathrm{i}}$ are amenable to simpler interpretation, and modeling, than the $D_{\mathrm{i,self}}$.

4.5 Degree of correlations for unary diffusion, $Đ_{\mathrm{i}}/Đ_{\mathrm{ii}}$

It is convenient to define the degree of correlations for unary diffusion in microporous materials, as $\frac{Đ_i}{Đ_{ii}}$. In view of Equation (S19) we get

$$\frac{Đ_i}{Đ_{ii}}=\frac{Đ_i}{D_{i,self}}-1;\quad D_{i,self}=\frac{Đ_i}{1+\frac{Đ_i}{Đ_{ii}}} \tag{S21}$$

Equation (S21) shows that the degree of correlations can be determined from KMC simulations of $D_{\mathrm{i,self}}$ and $Đ_{\mathrm{i}}$. From Equation (S21) it can also be concluded that the self-diffusivity is always lower than the M-S diffusivity due to correlation effects. The larger the degree of correlations, $\frac{Đ_i}{Đ_{ii}}$, the lower is the value of $D_{\mathrm{i,self}}$ compared to $Đ_i$.

4.6 M-S formulation for binary mixture diffusion

For binary mixture diffusion in MFI zeolite, the Maxwell-Stefan equations (S1) are written

$$\begin{aligned} -\rho\frac{q_1}{RT}\frac{d\mu_1}{dz} &= \frac{x_2N_1 - x_1N_2}{Đ_{12}} + \frac{N_1}{Đ_1} \\ -\rho\frac{q_2}{RT}\frac{d\mu_2}{dz} &= \frac{x_1N_2 - x_2N_1}{Đ_{12}} + \frac{N_2}{Đ_2} \end{aligned} \tag{S22}$$

The first members on the right hand side of Equation (S22) are required to quantify slowing-down effects that characterize binary mixture diffusion.[2, 11, 17] There is no experimental technique for direct determination of the exchange coefficients $Đ_{12}$, that quantify molecule-molecule interactions.

In two-dimensional matrix notation, equation (S5) take the form

$$-\begin{pmatrix} \frac{q_1}{RT}\frac{d\mu_1}{dz} \\ \frac{q_2}{RT}\frac{d\mu_2}{dz} \end{pmatrix} = [\Gamma]\begin{pmatrix} \frac{dq_1}{dz} \\ \frac{dq_2}{dz} \end{pmatrix} \tag{S23}$$

For the mixed-gas Langmuir model, equation (S6), we can derive simple analytic expressions for the four elements of the matrix of thermodynamic factors:[18]

$$\begin{bmatrix} \Gamma_{11} & \Gamma_{12} \\ \Gamma_{21} & \Gamma_{22} \end{bmatrix} = \frac{1}{1-\theta_1-\theta_2}\begin{bmatrix} 1-\theta_2 & \theta_1 \\ \theta_2 & 1-\theta_1 \end{bmatrix} \tag{S24}$$

where the fractional occupancies, θ_i, are defined by equation (S6).

Let us define the square matrix [B]

$$[B] = \begin{bmatrix} \frac{1}{Đ_1} + \frac{x_2}{Đ_{12}} & -\frac{x_1}{Đ_{12}} \\ -\frac{x_2}{Đ_{12}} & \frac{1}{Đ_2} + \frac{x_1}{Đ_{12}} \end{bmatrix}; \quad [B]^{-1} = \frac{1}{1 + \frac{x_1Đ_2}{Đ_{12}} + \frac{x_2Đ_1}{Đ_{12}}}\begin{bmatrix} Đ_1\left(1 + \frac{x_1Đ_2}{Đ_{12}}\right) & \frac{x_1Đ_1Đ_2}{Đ_{12}} \\ \frac{x_2Đ_1Đ_2}{Đ_{12}} & Đ_2\left(1 + \frac{x_2Đ_1}{Đ_{12}}\right) \end{bmatrix} \tag{S25}$$

In proceeding further, it is convenient to define a 2×2 dimensional square matrix $[\Lambda] \equiv [B]^{-1}$:

$$[\Lambda]=\begin{bmatrix}\frac{1}{Đ_1}+\frac{x_2}{Đ_{12}} & -\frac{x_1}{Đ_{12}}\\ -\frac{x_2}{Đ_{12}} & \frac{1}{Đ_2}+\frac{x_1}{Đ_{12}}\end{bmatrix}^{-1}=\frac{1}{1+\frac{x_1Đ_2}{Đ_{12}}+\frac{x_2Đ_1}{Đ_{12}}}\begin{bmatrix}Đ_1\left(1+\frac{x_1Đ_2}{Đ_{12}}\right) & \frac{x_1Đ_1Đ_2}{Đ_{12}}\\ \frac{x_2Đ_1Đ_2}{Đ_{12}} & Đ_2\left(1+\frac{x_2Đ_1}{Đ_{12}}\right)\end{bmatrix} \tag{S26}$$

Equation (S22) can be re-cast into 2-dimensional matrix notation

$$(N)=-\rho[\Lambda][\Gamma]\frac{d(q)}{dz};$$

$$\begin{pmatrix}N_1\\ N_2\end{pmatrix}=-\frac{\rho}{1+\frac{x_1Đ_2}{Đ_{12}}+\frac{x_2Đ_1}{Đ_{12}}}\begin{bmatrix}Đ_1\left(1+\frac{x_1Đ_2}{Đ_{12}}\right) & \frac{x_1Đ_1Đ_2}{Đ_{12}}\\ \frac{x_2Đ_1Đ_2}{Đ_{12}} & Đ_2\left(1+\frac{x_2Đ_1}{Đ_{12}}\right)\end{bmatrix}\begin{bmatrix}\Gamma_{11} & \Gamma_{12}\\ \Gamma_{21} & \Gamma_{22}\end{bmatrix}\begin{pmatrix}\frac{dq_1}{dz}\\ \frac{dq_2}{dz}\end{pmatrix} \tag{S27}$$

The elements of $[B]$ can be obtained by inverting the matrix $[\Lambda]$ determined using MD simulations using equation (S13):

$$\begin{bmatrix}B_{11} & B_{12}\\ B_{21} & B_{22}\end{bmatrix}=\begin{bmatrix}\frac{1}{Đ_1}+\frac{x_2}{Đ_{12}} & -\frac{x_1}{Đ_{12}}\\ -\frac{x_2}{Đ_{12}} & \frac{1}{Đ_2}+\frac{x_1}{Đ_{12}}\end{bmatrix}=[\Lambda]^{-1} \tag{S28}$$

The three M-S diffusivities can be backed-out from the four elements $\begin{bmatrix}B_{11} & B_{12}\\ B_{21} & B_{22}\end{bmatrix}$ using;

$$Đ_{12}=-\frac{x_1}{B_{12}}=-\frac{x_2}{B_{21}};\quad Đ_1=\frac{1}{B_{11}-\frac{x_2}{Đ_{12}}};\quad Đ_2=\frac{1}{B_{22}-\frac{x_1}{Đ_{12}}} \tag{S29}$$

4.7 Occupancy Dependence of unary M-S diffusivity

The simplest model to describe this occupancy dependence is

$$Đ_i=Đ_i(0)(1-\theta)=Đ_i(0)\theta_V \tag{S30}$$

where $Đ_i(0)$ is the M-S diffusivity at "zero-loading", and $\theta_V=(1-\theta)$ is the fractional vacancy. Equation (S30) is essentially based on a simple hopping model in which a molecule can jump from one

adsorption site to an adjacent one, provided it is not already occupied. The loading dependence portrayed in equation (S30) has been termed the "strong confinement" scenario by Krishna and Baur.[18]

For the specific case of a binary mixture, the hopping of molecules from one site to another on a 2D lattice is depicted in Figure S9. Using a simple lattice model, the M-S diffusivity in the limit of vanishingly small occupancies, $Đ_i(0) = \frac{1}{\zeta}\nu_i(0)\lambda^2$, where $\zeta = 4$ is the coordination number of the 2D array of lattice sites, λ is the jump distance on the square lattice, and $\nu_i(0)$ is the jump frequency at vanishingly small occupancy.[19]

More generally, molecule-molecule interactions serve to influence the jump frequencies by a factor that depends on the energy of interaction, *w*. For repulsive interactions, $w > 0$, whereas for attractive interactions, $w < 0$. Using the quasi-chemical approach of Reed and Ehrlich[20] to quantify such interactions, the following expression is obtained for the occupancy dependence of the M-S diffusivities [19, 21, 22]

$$Đ_i = Đ_i(0)\left(\frac{1+\beta_i}{2\,(1-\theta_i)}\right)^{-\zeta}\left(1+\frac{(\beta_i - 1 + 2\theta_i)\phi}{2\,(1-\theta_i)}\right)^{\zeta-1} \tag{S31}$$

In equation (S31) the following dimensionless parameters are defined

$$\beta_i = \sqrt{1-4\,\theta_i(1-\theta_i)(1-1/\phi)}; \quad \phi = \exp(w/RT) \tag{S32}$$

In the limiting case of negligible molecule-molecule interactions, $w = 0$, $\phi = 1$, $\beta_i = 1$ equation (S31) degenerates to yield Equation (S30).

4.8 List of Figures for The Maxwell-Stefan formulation for diffusion in micropores

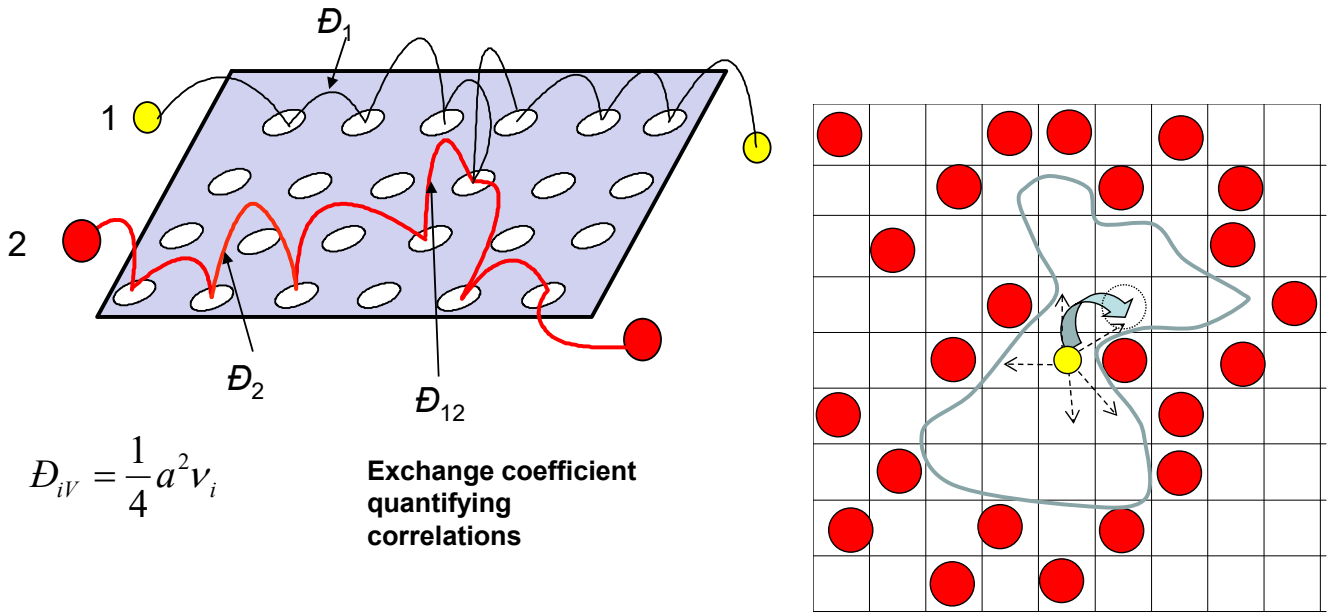

$$Đ_{iV} = \frac{1}{4} a^2 \nu_i$$

Figure S9. The Maxwell- Stefan description of hopping of molecules on a 2D surface.

5 Kinetic Monte Carlo (KMC) simulations

5.1 KMC simulation methodology

The Kinetic Monte Carlo (KMC) simulation methodology is detailed in earlier publications.[21, 23-29] A brief outline is provided below for the methodology as applied to the diffusion of propane (C3) n-butane (nC4), and iso-butane (iC4) in MFI zeolite. Configurational-Bias Monte Carlo (CBMC) simulation data for the unary isotherms of C3, nC4, and iC4 at 300 K, and 363 K are shown in Figure S10(a,b); the unary isotherm fit parameters are provided in Table S1, and Table S2. The saturation capacities of these three guest molecules lie in the range 10 – 12 molecules per unit cell. MD simulations of the loading dependence of the M-S diffusivities of C3 and nC4 show a near linear decrease in diffusivity as the loading increases to 12 molecules per unit cell; see Figure S10(c). CBMC simulations of the isosteric heats of adsorption of nC4 and iC4 are presented in Figure S10(d); the isosteric heats of adsorption, Q_{st}, of nC4 and iC4 are close to each other, in line with available experimental data.[30] Also, for both nC4 and iC4, the values of Q_{st}, are practically independent of loading, suggesting that molecule-molecule attraction and repulsions are not significant; rather the molecule-wall interactions are dominant.

The CBMC and MD data in Figure S10 suggests that the total number of adsorption sites for C3, nC4 and iC4 is 12 per unit cell. Therefore, the MFI lattice topology (see Figure S11) is made up of equal sized sorption sites, 12 in total, distributed along the straight channels (4, marked green), zig-zag channels (4, marked blue) and at the intersections (4, marked red). A total of 2×2×4 = 16 unit cells were used in all of the simulations reported in this work; see Figure S12. In the 2×2×4 unit cells, there are a total of 64 intersection sites. In the KMC simulations we assume that the each site can be occupied by only one molecule at a time. Particles can move from one site to a neighboring site via hops. Let ν_{str} and ν_{zz} denote the jump frequencies along the straight and zig-zag channels when moving *towards* the intersections. Based on MD simulations it is concluded that the frequencies along the straight channels

is greater than along the zig-zag channels $\nu_{str} > \nu_{zz}$.[23-25] As illustration, Figure S13 shows MD simulation data of self-diffusivities of linear alkanes (methane (C1), ethane (C2), propane (C4), n-butane (nC4)), in *x*-, *y*-, *z*- directions for diffusion of four different binary mixtures of varying compositions in MFI zeolite at total loading of $\Theta = 4$ molecules uc^{-1}. We note that in each case the self-diffusivity in the *z*- direction (i.e. along the straight channels) is about a factor 2 higher than the self-diffusivity in x*z*- direction. The preferential location of branched alkanes, such as iC4, at the intersection sites can be modelled by taking the jump frequencies away from the intersection sites to be lower, by a factor *f*, than the corresponding frequencies ν_{str}, and ν_{zz}. Typically for intersection blocking, *f*, has the value of the order of 0.001 – 0.0001.

A standard KMC methodology to propagate the system was employed.[23, 24, 31-34] A hop is made every KMC step and the system clock is updated with variable time steps. For a given configuration of random walkers on the lattice a process list containing all possible *M* moves to vacant intersection sites is created. Each possible move *i* is associated with a jump probability ν_i. Note that the values depend on the particular type a particle belongs to, as well as on the possible occupation of neighbouring sites. The *mean* elapsed time τ is the inverse of the total rate coefficient $\tau^{-1} = \nu_{total} = \sum_{i=1}^{M} \nu_i$ which is then determined as the sum over all processes contained in the process list. The actual KMC time step Δt for a given configuration is randomly chosen from a Poisson distribution $\Delta t = -\ln(u)/\nu_{total}$ where $u \in [0,1]$ is a uniform random deviate. The time step Δt is independent from the chosen hopping process. To select the actual jump, we define process probabilities according to $p_i = \sum_{j=1}^{i} \nu_j / \nu_{total}$. The *i*th process is chosen, when $p_{i-1} < \upsilon < p_i$, where $\upsilon \in [0,1]$ is another uniform random deviate. After having performed a hop, the process list is updated. In order to avoid wall effects we employ periodic boundary conditions.

Kinetic Monte Carlo (KMC) simulations

In order to account for nearest neighbour interactions, the transition rates have to be altered if another particle occupies an adjacent site. The employed procedure is illustrated in Figure S14. It is based on the assumption that the logarithm of the hopping rate is proportional to the relative height of the energy barrier, as for example given by $E_{trans} - E_A$ for the move from A to B. Consider two neighboring particles at positions A and B. In order to ensure energy conservation, both particles have to experience the same repulsive interaction δE_{AB}. The depth of the potential well of a particle at position A is modified by δE_A, which is determined by summing over all possible nearest-neighbor interactions $\delta E_A = \sum_B \delta E_{AB}$. Here B indicates all *occupied* nearest neighbor positions with respect to A. In the KMC scheme the rates of all possible moves of the particle located at A have to be changed by a factor $\nu'_{A\to B'} = \nu_{A\to B'} \exp(\frac{\delta E_A}{RT})$. Here B' denotes all empty nearest neighbour positions with respect to A. Since we do not wish to introduce an explicit value for the temperature T in our KMC development, the Arrhenius term is replaced by a product of pair-pair interaction factors ϕ_{AB} $\nu'_{A\to B'} = \nu_{A\to B'} \prod_B \phi_{AB}$ with $\phi_{AB} = \phi = \exp(\frac{\delta E_{AB}}{RT})$. The parameter ϕ is directly relatable to the interaction parameter defined in the Reed-Ehrlich model in equations (S31), and (S32), as explained in detail in our earlier works.[19, 21]

Since only nearest neighbor interactions are involved, the scheme is simple and the computational effort is moderate. The influence of the pair-pair interaction factors ϕ set equal to 1 (no repulsions), or > 1 (finite repulsion). The value of ϕ can be chosen to match experimental or MD simulation data. MD simulations of the loading dependence of the M-S diffusivities of C3 and nC4 show a near linear decrease in diffusivity as the loading increases to 12 molecules per unit cell; see Figure S10(c). This linear reduction is in line with the simple model described by Equation (S30). Consequently, the interaction parameter ϕ for C3 and nC4 is taken to be unity in all of the KMC simulations reported here.

Kinetic Monte Carlo (KMC) simulations

The unary Maxwell-Stefan diffusivities $Đ_i$ are obtained from molecular displacements using the formula in each of the coordinate direction

$$Đ_i = \frac{1}{2}\lim_{\Delta t\to\infty}\frac{1}{n_i}\frac{1}{\Delta t}\left\langle\left(\sum_{l=1}^{n_i}\left(\mathbf{r}_{l,i}(t+\Delta t)-\mathbf{r}_{l,i}(t)\right)\right)^2\right\rangle \tag{S33}$$

In this expression n_i represents the number of molecules of species *i*, and $\mathbf{r}_{l,i}(t)$ is the position of molecule *l* of species *i* at any time *t*.

The unary self-diffusivities $D_{i,self}$ are computed by analyzing the mean square displacement of each species *i* for each coordinate direction

$$D_{i,self} = \frac{1}{2n_i}\lim_{\Delta t\to\infty}\frac{1}{\Delta t}\left\langle\left(\sum_{l=1}^{n_i}\left(\mathbf{r}_{l,i}(t+\Delta t)-\mathbf{r}_{l,i}(t)\right)^2\right)\right\rangle \tag{S34}$$

For binary mixtures, the four elements of the Maxwell-Stefan matrix Λ_{ij} are accessible from KMC simulations[21, 23-29] by monitoring the individual molecular displacements

$$\Lambda_{ij} = \frac{1}{2}\lim_{\Delta t\to\infty}\frac{1}{n_j}\frac{1}{\Delta t}\left\langle\left(\sum_{l=1}^{n_i}\left(\mathbf{r}_{l,i}(t+\Delta t)-\mathbf{r}_{l,i}(t)\right)\right)\bullet\left(\sum_{k=1}^{n_j}\left(\mathbf{r}_{k,j}(t+\Delta t)-\mathbf{r}_{k,j}(t)\right)\right)\right\rangle \tag{S35}$$

In this expression n_i and n_j represent the number of molecules of species *i* and *j* respectively, and $\mathbf{r}_{l,i}(t)$ is the position of molecule *l* of species *i* at any time *t*.

Compliance with the Onsager Reciprocal Relations demands

$$n_j\Lambda_{ij} = n_i\Lambda_{ji};\quad i,j = 1,2,....n \tag{S36}$$

The M-S diffusivities $Đ_1, Đ_2$ are backed-out from Λ_{ij} using equations (S28), and (S29).

The KMC simulation methodology was implemented in a custom-built code, written in C++.

5.2 KMC simulations of iC4 diffusion in MFI zeolite at 298 K

Before proceeding with the analysis of nC4/iC4 mixture diffusion, we first demonstrate the ability of KMC simulations to capture the cusp-like dependence of the Maxwell-Stefan diffusivity, $Đ_i$, for iC4 diffusivity on the loading Θ_i as established in the Infra-Red Microscopy (IRM) experimental data of Chmelik et al.[29]; see Figure S15. Their data was measured at a temperature of 298 K.

Kinetic Monte Carlo (KMC) simulations

Figure S15(a) shows CBMC simulation data of the iC4 isotherm in MFI zeolite at 298 K; there is a distinct inflection at a loading Θ = 4 molecules/uc. The continuous solid lines are the dual-site Langmuir fits using the parameter values specified in Table S1. For iC4, the jumps *away* from the intersections towards either the straight or zig-zag channels occur at a frequency, lower by a factor *f*, because of the preference of iC4 to locate in the channel intersections. This factor *f* is determined by the ratio of the Langmuir constants in the Dual-site Langmuir fit of the unary iC4 isotherm

$$q = q_{A,sat}\frac{b_A p}{1+b_A p} + q_{B,sat}\frac{b_B p}{1+b_B p} \tag{S37}$$

From Table S1: $f = b_B / b_A = 2.87\times10^{-5} / 2.29\times10^{-2} = 0.0012$. The jump frequencies are chosen to match the zero-loading M-S diffusivity $Đ(0)$ = 1.2×10^{-12} m^2 s^{-1} in the experiments. On the basis of the IRM experiments of Chmelik et al.,[29] it is established that the transport along the zig-zig channels dominates the uptake process (See Supplementary Material of Chmelik et al.[29]), and it is the diffusivity along the *x*-direction that is of primary interest. The jump frequency along the zig-zag channels was chosen as $\nu_{zz} = 2\times10^9$ s^{-1}:

$\left(\nu_{str} = 3.5\times10^9 \text{ s}^{-1}; \nu_{zz} = 2\times10^9 \text{ s}^{-1}; f = 0.0012; f\nu_{str} = 4.2\times10^6 \text{ s}^{-1}; f\nu_{zz} = 2.4\times10^6 \text{ s}^{-1}\right)$.

The continuous solid lines in Figure S15(b) are the KMC simulations with different choices of the molecule-molecule repulsion/attraction parameters ϕ = 1, 2, 2.5 and 3. The KMC simulations are able to capture the essential characteristics of the loading dependence of iC4 in MFI. We note that the molecule-molecule interaction parameters are only relevant for iC4 loadings > 4 molecules uc^{-1}. For investigation of traffic junction effects, the maximum loading of iC4 is restricted to 4 molecules/uc, and therefore we take ϕ = 1 in all of the KMC simulations of iC4 diffusion.

5.3 KMC simulations of intersection blocking effects

Branched alkanes such as iC4, 2-methylpentane (2MP, and 2,2 dimethylbutane (22DMB) have diffusivities that are about three to four orders of magnitude below that of linear alkanes such as

propane (C3), n-butane (nC4). Consequently, the preferential location of branched alkanes at the intersection sites can be modelled by assuming that the intersections are blocked for molecular traffic.

In order to simulate the influence of intersection blocking, KMC simulations were also carried out in which a certain number of the total of 64 intersection sites in Figure S12 were blocked. The procedure for blocking is illustrated schematically in Figure S16 in which (a) 16 intersection sites are first selected, and (b) subsequently deleted, along with the connections to the adjoining straight and zig-zag channels.

A total of five different % blocking was employed:

(i) 6.25% = 4 intersection sites deleted

(ii) 12.5% = 8 intersection sites deleted

(iii) 25% = 16 intersection sites deleted

(iv) 37.5% = 24 intersection sites deleted

(v) 50% = 32 intersection sites deleted

Figure S17 presents the KMC simulation results for the influence of the degree of intersection blocking on M-S diffusivity, $Đ_1$, self-diffusivity, $D_{1,self}$ and degrees of correlation, $Đ_1/Đ_{11}$, for nC4 in MFI zeolite. The jump frequency values of nC4 $\left(\nu_{str} = 4\times10^{10}\ \text{s}^{-1}; \nu_{zz} = 2\times10^{10}\ \text{s}^{-1} f = 1; f\nu_{str} = 4\times10^{10}\ \text{s}^{-1}; f\nu_{zz} = 2\times10^{10}\ \text{s}^{-1}\right)$ are chosen to match the experimental self-diffusivity data of Fernandez et al.;[3] see Figure S3. It is interesting to note that the degree of correlations $Đ_1/Đ_{11}$ is independent of intersection blocking effects. The unary M-S diffusivities are well described by Equation (S30): $Đ_1 = Đ_1(0)\left(1-\theta\right)$, where the fractional occupancy θ is the total loading divided by the total number of available adsorption sites, after deletion of the selected number of intersection sites. For the unblocked topology, the zero-loading M-S diffusivity is $Đ_1(0) = 3.7\times10^{-9}\ \text{m}^2\text{s}^{-1}$. The zero-loading M-S diffusivity $Đ_1(0)$ decreases with the number of intersection sites blocked, $\Theta_{blocked}$, in one unit cell of MFI zeolite; see Figure S17(e). The KMC simulated data for the zero-loading diffusivities could be fitted as follows: $3.7\times10^{-9}\exp\left(-1.0\Theta_{blocked}\right)$.

The reduction in the zero-loading M-S diffusivity with increasing $\Theta_{blocked}$ is attributable to decrease in the connectivity of the MFI topology.

Figure S18 presents the KMC simulation results for the influence of intersection blocking on diffusion of propane (C3) in MFI zeolite. For C3, the jump frequencies are chosen to be twice that of nC4: $\left(\nu_{str} = 8\times10^{10}\ \text{s}^{-1}; \nu_{zz} = 4\times10^{10}\ \text{s}^{-1}; f = 1; f\nu_{str} = 8\times10^{10}\ \text{s}^{-1}; f\nu_{zz} = 4\times10^{10}\ \text{s}^{-1}\right)$. The KMC results are precisely analogous to that for nC4. For the unblocked topology, the zero-loading M-S diffusivity $Đ_1(0) = 7.4\times10^{-9}\ \text{m}^2\text{s}^{-1}$. The KMC simulated data for the zero-loading diffusivities could be fitted as follows: $7.4\times10^{-9}\exp\left(-1.0\Theta_{blocked}\right)$.

5.4 KMC simulations of nC4/iC4 mixture diffusion at 363 K

We analyze nC4/iC4 mixture diffusion in MFI at 363 K to compare with the experiments of Fernandez et al.[3] In these experiments the total mixture loading $\Theta_t = \Theta_1 + \Theta_2 = 4$ uc^{-1}. We assume negligible molecule-molecule repulsion or interactions, and set $\phi = 1$ for nC4, iC4, and nC4/iC4.

For iC4, the jumps *away* from the intersections towards either the straight or zig-zag channels occur at a frequency, lower by a factor *f*, because of the preference of iC4 to locate in the channel intersections. This factor *f* is determined by the ratio of the Langmuir constants in the Dual-site Langmuir fit parameters at 363 K from Table S2: $f = b_B / b_A = 8.02\times10^{-7} / 7.54\times10^{-4} = 0.001$; the arguments behind the choice of f are given in earlier publications.[26, 27, 29] The asymmetry in the jump frequencies towards and away from the intersections captures the inflection behavior of the sorption isotherm. These jump frequency values: $\left(\nu_{str} = 4\times10^{10}\ \text{s}^{-1}; \nu_{zz} = 2\times10^{10}\ \text{s}^{-1}; f = 0.001; f\nu_{str} = 4\times10^{7}\ \text{s}^{-1}; f\nu_{zz} = 2\times10^{7}\ \text{s}^{-1}\right)$ are chosen to match the experimental self-diffusivity data of Fernandez et al.;[3] see Figure S3.

For nC4, there are no perceptible isotherm inflections, and the jump frequencies towards, and away, from the intersection sites are equal to one another. The jump frequency along the zig-zag channels was chosen as $\nu_{zz} = 2\times10^{10}$ s^{-1}. The jump frequency along the straight channels is assumed to have a higher value $\nu_{str} = 4\times10^{10}$ s^{-1}. The jump frequency values of nC4

$\left(\nu_{str} = 4\times10^{10}\ \text{s}^{-1}; \nu_{zz} = 2\times10^{10}\ \text{s}^{-1}; f = 1; f\nu_{str} = 4\times10^{10}\ \text{s}^{-1}; f\nu_{zz} = 2\times10^{10}\ \text{s}^{-1}\right)$ are chosen to match the experimental self-diffusivity data of Fernandez et al.;[3] see Figure S3. The zero-loading M-S diffusivity is $Đ_1(0) = 3.7\times10^{-9}\ \text{m}^2\text{s}^{-1}$. At a loading of 4 molecules/uc, the M-S diffusivity of nC4 is $Đ_1 = 2.47\times10^{-9}\ \text{m}^2\text{s}^{-1}$.

Figure S19(a) presents the KMC simulations of unary M-S and self-diffusivities of nC4 (1) and iC4(2) as a function of loading, expressed as molecules per unit cell. The unary diffusivity of iC4 shows a linear decrease as the loading increases to 4 molecules per unit cell; further explanation of the loading dependences of iC4 diffusivities are provided in Chmelik et al.[29]

Figure S19(b) present the self-diffusivities of nC4(1) and iC4(2) for nC4/(1)/iC4(2) mixture diffusion (total loading is held constant at 4 molecules uc^{-1}), as function of the loading iC4 loading. The characteristics of the variation of the nC4 self-diffusivity with iC4 loading is analogous to that witnessed in the experimental data in Figure S3.

The persuasive reason for undertaking the KMC simulations is that M-S diffusivities can be backed-out from the KMC-simulated elements of the 2×2 dimensional square matrix $[\Lambda]$, using the same procedure as used earlier for MD simulations. The loading dependence of the M-S diffusivities, $Đ_1$ and $Đ_2$ are presented in Figure S19(c). Since the total loading is held constant at 4 molecules uc^{-1}, we should expect the M-S diffusivity of either component to be independent of the iC4 loading. The KMC simulations show a reduction in the magnitude of the M-S diffusivity by about two orders of magnitude. Figure S19(d) compares the KMC simulated M-S diffusivity of nC4 in the mixture, $Đ_1$, with the estimations based on the relation $2.47\times10^{-9}\exp\left(-1.0\Theta_{blocked}\right)$, that are based on the KMC simulations for nC4 in the blocked topologies in Figure S17. The important conclusion to be drawn from Figure S19(d) is that the reduction in the M-S diffusivity of nC4 in mixtures with increasing proportion of iC4 is not a consequence of correlation effects, but can be unequivocally attributable to loss of connectivity due to intersection blocking.

Kinetic Monte Carlo (KMC) simulations

A different way to demonstrate that intersection blocking effects is to analyze diffusion of equimolar ($\Theta_1 = \Theta_2$) nC4(1)/iC4(2) mixtures with varying total loadings. Figure S20(a, b) present KMC simulation data for self- and M-S diffusivities of nC4 (1) and iC4(2) for nC4(1)/iC4(2) mixture diffusion for equimolar ($\Theta_1 = \Theta_2$) mixtures, as function of the total loading $\Theta_t = \Theta_1 + \Theta_2$; in these KMC simulations, the jump frequencies for iC4 are: $\left(\nu_{str} = 4\times10^{10}\ \text{s}^{-1}; \nu_{zz} = 2\times10^{10}\ \text{s}^{-1}; f = 0.001; f\nu_{str} = 4\times10^{7}\ \text{s}^{-1}; f\nu_{zz} = 2\times10^{7}\ \text{s}^{-1}\right)$. Compared to the unary diffusivities, we note that both self- and M-S diffusivities for nC4 are reduced by about two orders of magnitude due to intersection blocking by iC4.

5.5 KMC simulations of nC4/2MP mixture diffusion

We also conducted KMC simulations for nC4/2MP mixtures presented in which the jump frequencies for 2MP are taken to be $\left(\nu_{str} = 4\times10^{9}\ \text{s}^{-1}; \nu_{zz} = 2\times10^{9}\ \text{s}^{-1}; f = 0.001; f\nu_{str} = 4\times10^{6}\ \text{s}^{-1}; f\nu_{zz} = 2\times10^{6}\ \text{s}^{-1}\right)$, a factor 10 lower than those for iC4. Figure S21 shows that both the self-diffusivity and M-S diffusivity of nC4 in the mixture is practically independent of the partner species, iC4 or 2MP.

5.6 KMC simulations of C3/iC4 mixture diffusion

Figure S22 compares the KMC simulations for self- diffusivities of nC4/iC4 and C3/iC4 mixture diffusion (total loading is held constant at 4 molecules uc^{-1}), as function of the loading of iC4. In these simulations, the jump frequencies for C3 (propane) is taken as $\left(\nu_{str} = 8\times10^{10}\ \text{s}^{-1}; \nu_{zz} = 4\times10^{10}\ \text{s}^{-1}; f = 1; f\nu_{str} = 8\times10^{10}\ \text{s}^{-1}; f\nu_{zz} = 4\times10^{10}\ \text{s}^{-1}\right)$, a factor 2 higher than those for nC4. The results show that the choice of the jump frequencies of the linear alkane have only a small influence on the self-diffusivities of iC4. Furthermore, we note that the influence of intersection blocking by iC4 is to reduce the self-diffusivities and M-S diffusivities of C3 and nC4 to the same extent, and in analogous manners.

5.7 Contrasting intersection blocking with correlation effects

In order to highlight the sharp constrasts between intersection blocking effects as witnessed in the KMC simulations presented in Figure S19, Figure S20, Figure S21, and Figure S22 with the usual correlation effects we performed KMC simulations for nC4 mixed with a "hypothetical" guest species iC4* in which the jump frequencies for iC4* are prescribed as $\left(\nu_{str} = 4\times10^{7}\ \text{s}^{-1}; \nu_{zz} = 2\times10^{7}\ \text{s}^{-1}; f = 1; f\nu_{str} = 4\times10^{7}\ \text{s}^{-1}; f\nu_{zz} = 2\times10^{7}\ \text{s}^{-1}\right)$; this implies that there is no preference for iC4* to locate at the intersections. Therefore, neither guest species has preference for any of the adsorption sites, and there are no traffic junction effects in play for this mixture. For nC4 the chosen jump frequencies are $\left(\nu_{str} = 4\times10^{10}\ \text{s}^{-1}; \nu_{zz} = 2\times10^{10}\ \text{s}^{-1}; f = 1; f\nu_{str} = 4\times10^{10}\ \text{s}^{-1}; f\nu_{zz} = 2\times10^{10}\ \text{s}^{-1}\right)$. The KMC simulations for unary nC4, unary iC4*, and equimolar ($\Theta_1 = \Theta_2$) nC4/iC4* mixtures are summarized in Figure S23.

The unary M-S diffusivities are well described by Equation (S30) with $\begin{matrix}\textbf{Component 1 = nC4}\\ Đ_1(0) = 3.7\times10^{-9}\ \text{m}^2\text{s}^{-1}\\ \textbf{Component 2 = iC4*}\\ Đ_2(0) = 3.6\times10^{-12}\ \text{m}^2\text{s}^{-1}\end{matrix}$; see Figure S23(c). The degree of self-correlations for unary diffusion are fitted as $\begin{matrix}\textbf{Component 1 = nC4}\\ Đ_1/Đ_{11} = b_1\theta^2;\quad b_1 = 2.8\\ \textbf{Component 2 = iC4*}\\ Đ_2/Đ_{22} = b_2\theta;\quad b_2 = 1\end{matrix}$; see Figure S25(d). The unary self-diffusivities predicted by $D_{i,self} = \dfrac{Đ_i}{1+\dfrac{Đ_i}{Đ_{ii}}}$ are in good agreement with the KMC simulated self-diffusivities; see Figure S23(e).

The M-S diffusivities backed out from KMC equimolar ($\Theta_1 = \Theta_2$) nC4/iC4* mixture simulations are in good agreement with the unary diffusivities of nC4, and iC4* when compared at the same occupancy as in the mixture; see Figure S23(f). When there are no intersection blocking effects, the M-S diffusivity for mixture diffusion has the same magnitude as the unary diffusivity, when compared at the same

occupancy within the MFI zeolite. For nC4/iC4*mixtures, the self-diffusivity of nC4 in the mixture is lowered below the value of the unary self-diffusivity, $D_{1,self}$, by a factor of about three; see Figure S23(g).

The KMC results for equimolar ($\Theta_1 = \Theta_2$) nC4/iC4* mixtures should be contrasted with the corresponding KMC simulation results presented in Figure S20(a, b) for self- and M-S diffusivities of nC4 (1) and iC4(2) for nC4/(1)/iC4(2) mixtures in which the preferential location of iC4 at the intersections are properly accounted by the choice: $\left(\nu_{str} = 4\times10^{10}\ \text{s}^{-1}; \nu_{zz} = 2\times10^{10}\ \text{s}^{-1}; f = 0.001; f\nu_{str} = 4\times10^{7}\ \text{s}^{-1}; f\nu_{zz} = 2\times10^{7}\ \text{s}^{-1}\right)$. Compared to the unary diffusivities, we note that *both* the M-S and self-diffusivities for nC4 are reduced by about two orders of magnitude with increased pore occupancies.

A different demonstration of the differences between intersection blocking effects and correlation effects is presented by the KMC simulation results for nC4/iC4 and nC4/iC4* mixtures for which the total loading ($\Theta_1 + \Theta_2$) is held constant at 4 molecules/uc. Figure S24(a,b,c,d) compare the KMC simulations for self-diffusivities in nC4/iC4 mixtures with those of nC4 mixed with a "hypothetical" guest species iC4* that has no preference to locate at the intersections. The nC4/iC4* mixture should be expected to be subject to the "normal" correlation effects. Indeed, the self-diffusivity of nC4 is reduced by a factor of about three with increasing proportion of the tardier hypothetical partner iC4* in the mixture. In contrast, intersection blocking effects for iC4 (with jump frequencies: $\left(\nu_{str} = 4\times10^{10}\ \text{s}^{-1}; \nu_{zz} = 2\times10^{10}\ \text{s}^{-1}; f = 0.001; f\nu_{str} = 4\times10^{7}\ \text{s}^{-1}; f\nu_{zz} = 2\times10^{7}\ \text{s}^{-1}\right)$), has the effect of reducing the nC4 self-diffusivity by about three orders of magnitude.

KMC simulations of the M-S diffusivities for nC4/iC4, and nC4/iC4* mixtures are plotted in Figure S24(e,f). As is to be expected, when there is no intersection blocking by the hypothetical iC4*, the M-S diffusivities of both nC4 and iC4* are independent of loading. For intersection blocking with nC4/iC4 mixtures, the M-S diffusivity of nC4 is reduced by about two orders of magnitude with increasing proportion of iC4 in the mixture.

5.8 KMC simulations of C3/nC4 mixture diffusion without traffic junction effects

In order to highlight the sharp constrast between the strong influence of traffic junction effects as witnessed in the KMC simulations presented in Figure S19, Figure S20, Figure S21, and Figure S22 with the usual correlation effects we performed KMC simulations for C3/nC4 mixtures in which neither guest species has preference for any of the adsorption sites, and there are no traffic junction effects. For C3 (propane) the jump frequencies are:

$\left(\nu_{str} = 8\times10^{10}\ \text{s}^{-1}; \nu_{zz} = 4\times10^{10}\ \text{s}^{-1}; f = 1; f\nu_{str} = 8\times10^{10}\ \text{s}^{-1}; f\nu_{zz} = 4\times10^{10}\ \text{s}^{-1}\right)$, and for nC4 the chosen jump frequencies are $\left(\nu_{str} = 4\times10^{10}\ \text{s}^{-1}; \nu_{zz} = 2\times10^{10}\ \text{s}^{-1}; f = 1; f\nu_{str} = 4\times10^{10}\ \text{s}^{-1}; f\nu_{zz} = 2\times10^{10}\ \text{s}^{-1}\right)$. The KMC simulations for unary C3, unary nC4, and equimolar ($\Theta_1 = \Theta_2$) C3/nC4 mixtures are summarized in Figure S25. The unary M-S diffusivities are well described by Equation (S30) with

$$\begin{matrix}\textbf{Component 1} = \textbf{C}_3\textbf{H}_8 \\ Đ_1(0) = 7.4\times10^{-9}\ \text{m}^2\text{s}^{-1} \\ \textbf{Component } 2 = n\textbf{C}_4\textbf{H}_{10} \\ Đ_1(0) = 3.7\times10^{-9}\ \text{m}^2\text{s}^{-1}\end{matrix}$$

; see Figure S25(c). The degree of self-correlations for unary diffusion are fitted as

$$\begin{matrix}\textbf{Component 1} = \textbf{C}_3\textbf{H}_8 \\ Đ_1/Đ_{11} = b_1\theta^2; \quad b_1 = 2.8 \\ \textbf{Component } 2 = n\textbf{C}_4\textbf{H}_{10} \\ Đ_2/Đ_{22} = b_2\theta^2; \quad b_2 = 2.8\end{matrix}$$

; see Figure S25(d). The unary self-diffusivities predicted by $D_{i,self} = \dfrac{Đ_i}{1+\dfrac{Đ_i}{Đ_{ii}}}$ are in good agreement with the KMC simulated self-diffusivities; see Figure S25(e).

The exchange coefficient for binary mixture diffusion, $Đ_{12}$ can be estimated using the interpolation formula

$$Đ_{12} = (Đ_{11})^{x_1}(Đ_{22})^{x_2} \tag{S38}$$

Figure S25(e) compares the estimates of $\Lambda_{11}, \Lambda_{22}$ with estimates from equation (S26) using the fits the unary M-S diffusivities $Đ_1, Đ_2$, along with the interpolation formula (S38). The *x*-axis in Figure S25(e)

is the mixture occupancy, which is the total mixture loading divided by the saturation capacity of 12 molecules per unit cell. There is good agreement of the Maxwell-Stefan model and the KMC simulated values of $\Lambda_{11}, \Lambda_{22}$.

A different demonstration of the applicability of the Maxwell-Stefan formulation is to compare the backed out M-S diffusivities $Đ_1, Đ_2$ from KMC simulated Λ_{ij} using equations (S28), and (S29). The M-S diffusivities backed out from KMC mixture simulations are in good agreement with the unary diffusivities of C3, and nC4 when compared at the same occupancy as in the mixture; see Figure S25(g). When there are no intersection blocking effects, the M-S diffusivity for mixture diffusion has the same magnitude as the unary diffusivity, when compared at the same occupancy within the MFI zeolite. This conclusion should be contrasted with those presented in KMC simulations presented in Figure S19, Figure S21, and Figure S22 wherein there is a reduction in the M-S diffusivity in mixtues with increased loading of the branched alkane partners.

Figure S25(h) compares the self-diffusivities in the mixture with the corresponding unary self-diffusivities at the same occupancy. The self-diffusivity of the more mobile C3 in the mixture is slightly lowered due to correlations with the tardier nC4.

5.9 List of Tables for Kinetic Monte Carlo (KMC) simulations

Table S1. Dual-site Langmuir-Freundlich parameters for guest molecules in MFI at 300 K. To convert from molecules uc^{-1} to mol kg^{-1}, multiply by 0.173367.

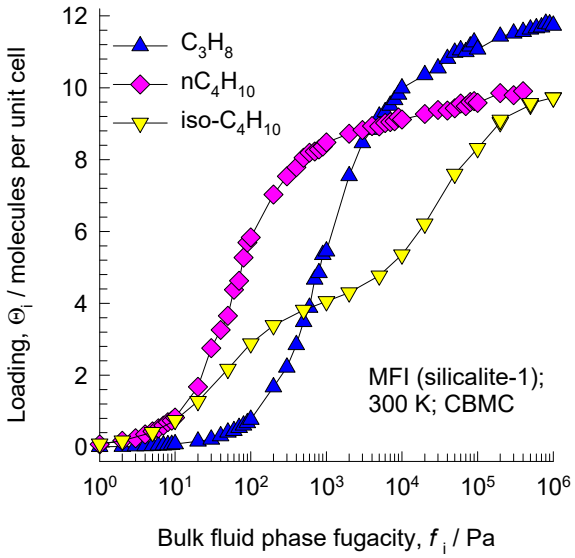

	Site A			Site B		
	$\Theta_{A,sat}$ molecules uc^{-1}	b_A $Pa^{-\nu_A}$	ν_A dimensionless	$\Theta_{B,sat}$ molecules uc^{-1}	b_B $Pa^{-\nu_A}$	ν_B dimensionless
C3H8	1.4	3.35E-04	0.67	10.7	6.34E-04	1.06
nC4H10	1.5	2.24E-03	0.57	8.7	9.75E-03	1.12
iso-C4H10	4	2.29E-02	1	6	2.87E-05	1

Table S2. Dual-site Langmuir-Freundlich parameters for guest molecules in MFI at 363 K. To convert from molecules uc^{-1} to mol kg^{-1}, multiply by 0.173367.

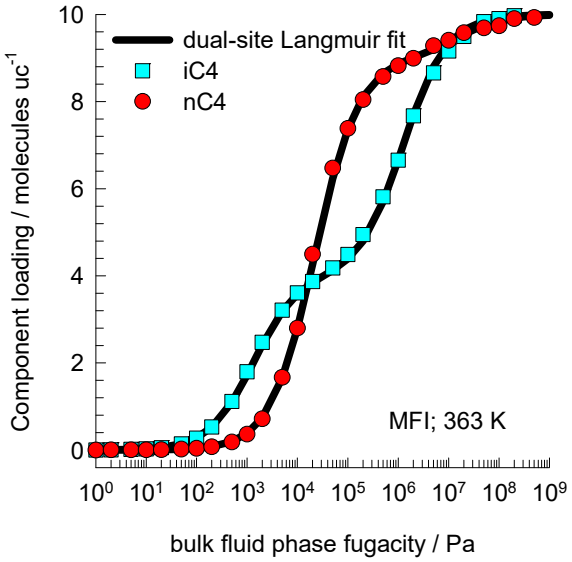

	Site A			Site B		
	$\Theta_{A,sat}$ molecules uc^{-1}	b_A $Pa^{-\nu_A}$	ν_A dimensionless	$\Theta_{B,sat}$ molecules uc^{-1}	b_B $Pa^{-\nu_B}$	ν_B dimensionless
nC4H10	1	6.2E-08	1	9	4.48E-05	1
isoC4H10	4	7.54E-04	1	6	8.02E-07	1

5.10 List of Figures for Kinetic Monte Carlo (KMC) simulations

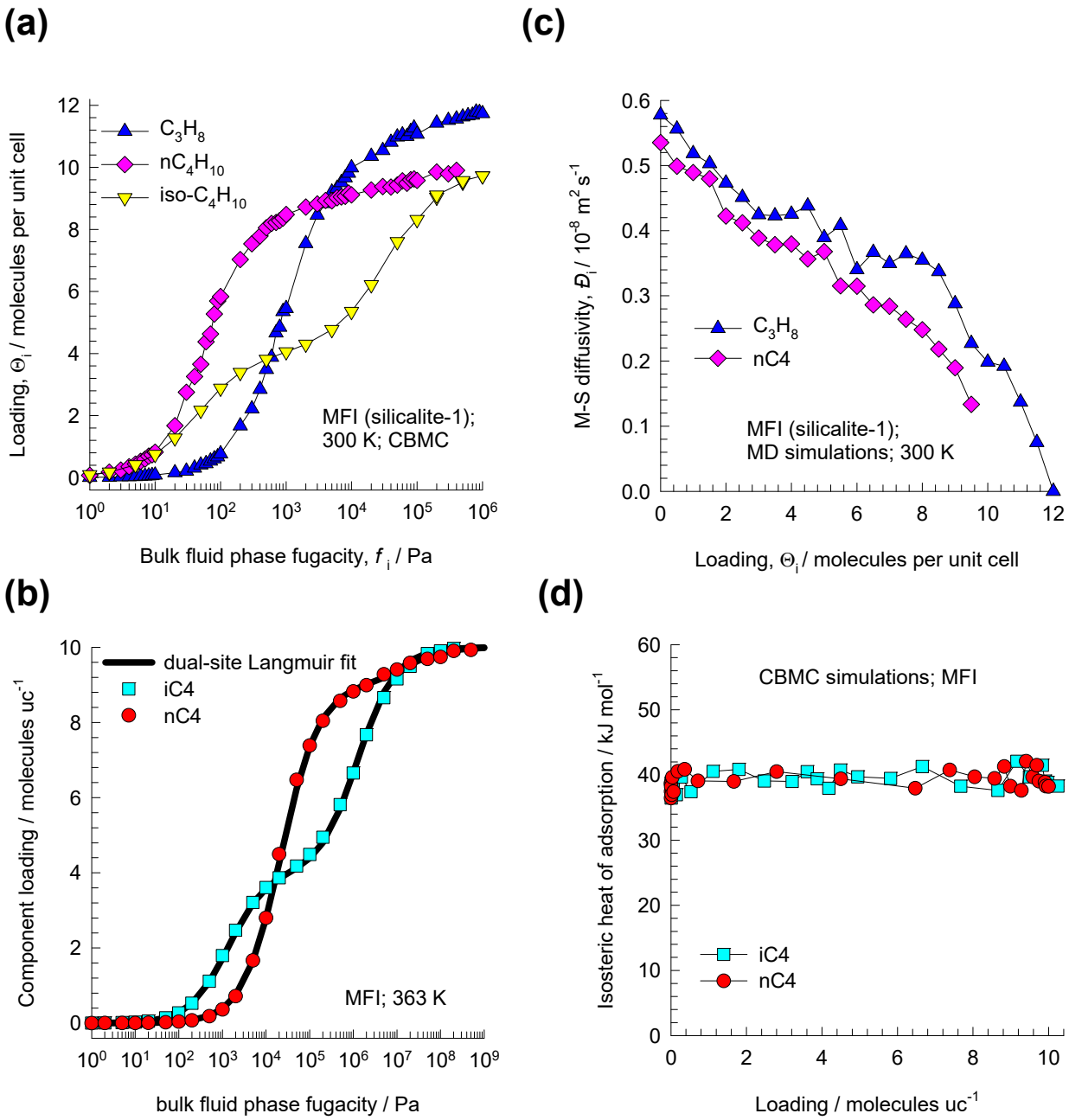

Figure S10. (a, b) CBMC simulations[3, 35] of the unary isotherms of C3, nC4, and iC4 at (a) 300 K, and (b) 363 K in MFI zeolite. (c) MD simulations of the Maxwell-Stefan diffusivity of C3, and nC4 in MFI at 300 K.[35] (d) CBMC simulations of the isosteric heats of adsorption of , nC4, and iC4 in MFI zeolite; these simulations are culled from earlier works.[36, 37]

Kinetic Monte Carlo (KMC) simulations

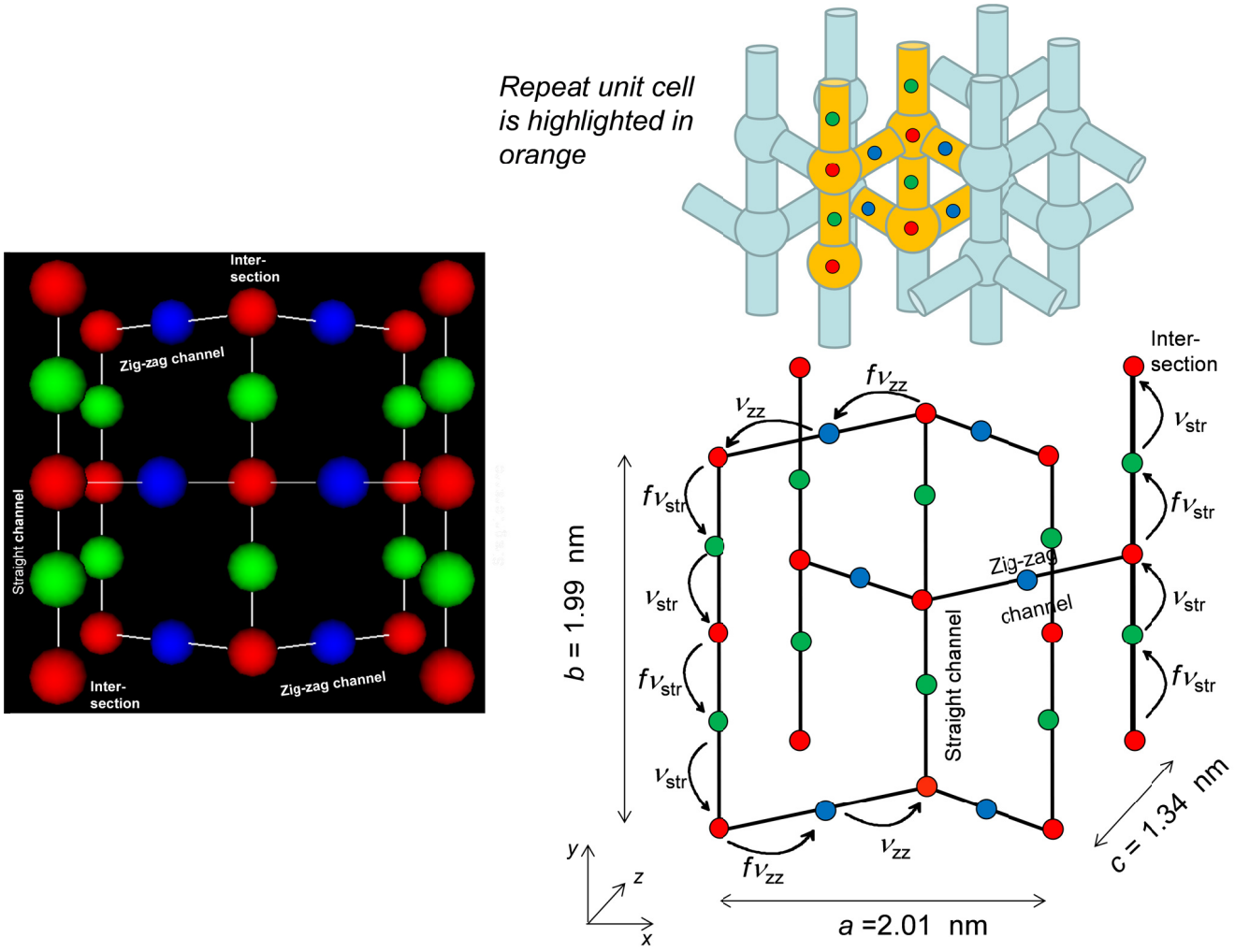

Figure S11. KMC simulation strategy for MFI topology. The total number of adsorption sites is 12, distributed as shown.

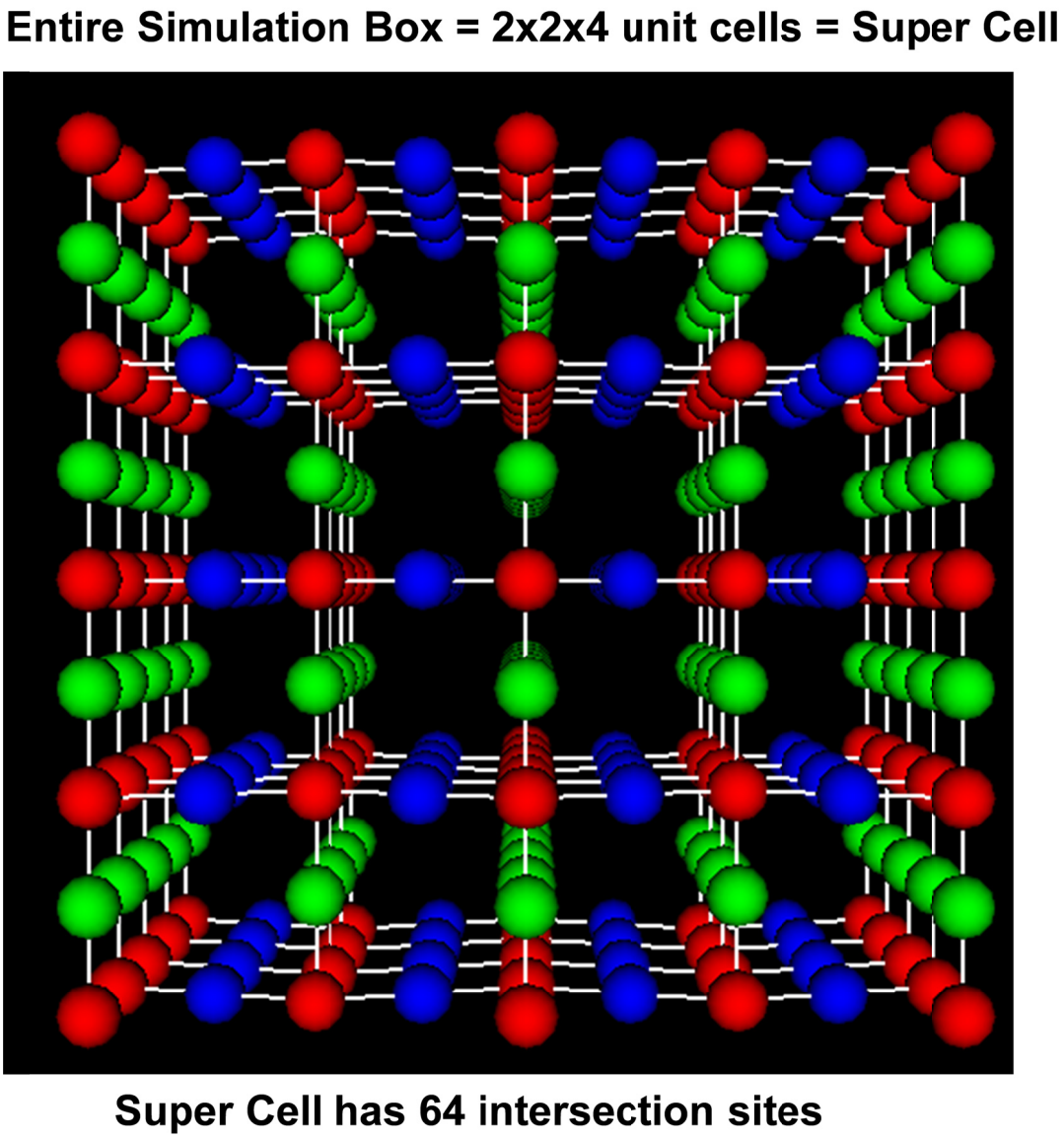

Figure S12. The total simulation box (= Super Cell) consisting of 2×2×4 unit cells of MFI zeolite. The total number of adsorption sites is 192. The total number of intersection sites in the Super Cell is 64 distributed as shown.

Kinetic Monte Carlo (KMC) simulations

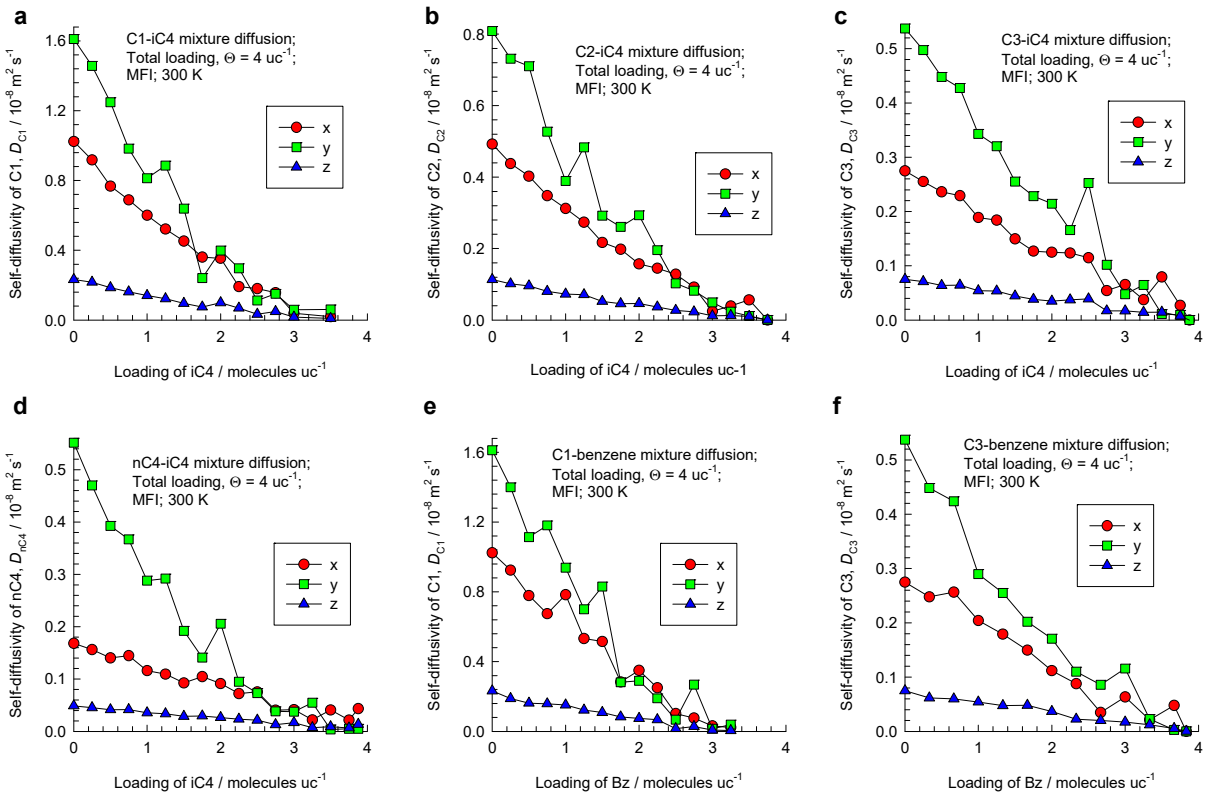

Figure S13. Molecular Dynamics (MD) simulations of self-diffusivities of linear alkanes (methane (C1), ethane (C2), propane (C4), n-butane (nC4)), in *x*-, *y*-, *z*- directions for diffusion of binary mixtures of varying compositions: (a) C1/iC4, (b) C2/iC4, (c) C3/iC4, (d) nC4/iC4, (e) C1/benzene, and (f) C3/benzene in MFI zeolite at total loading of $\Theta = 4$ molecules uc^{-1}. The MD simulation data are culled from previous work.[38]

Kinetic Monte Carlo (KMC) simulations

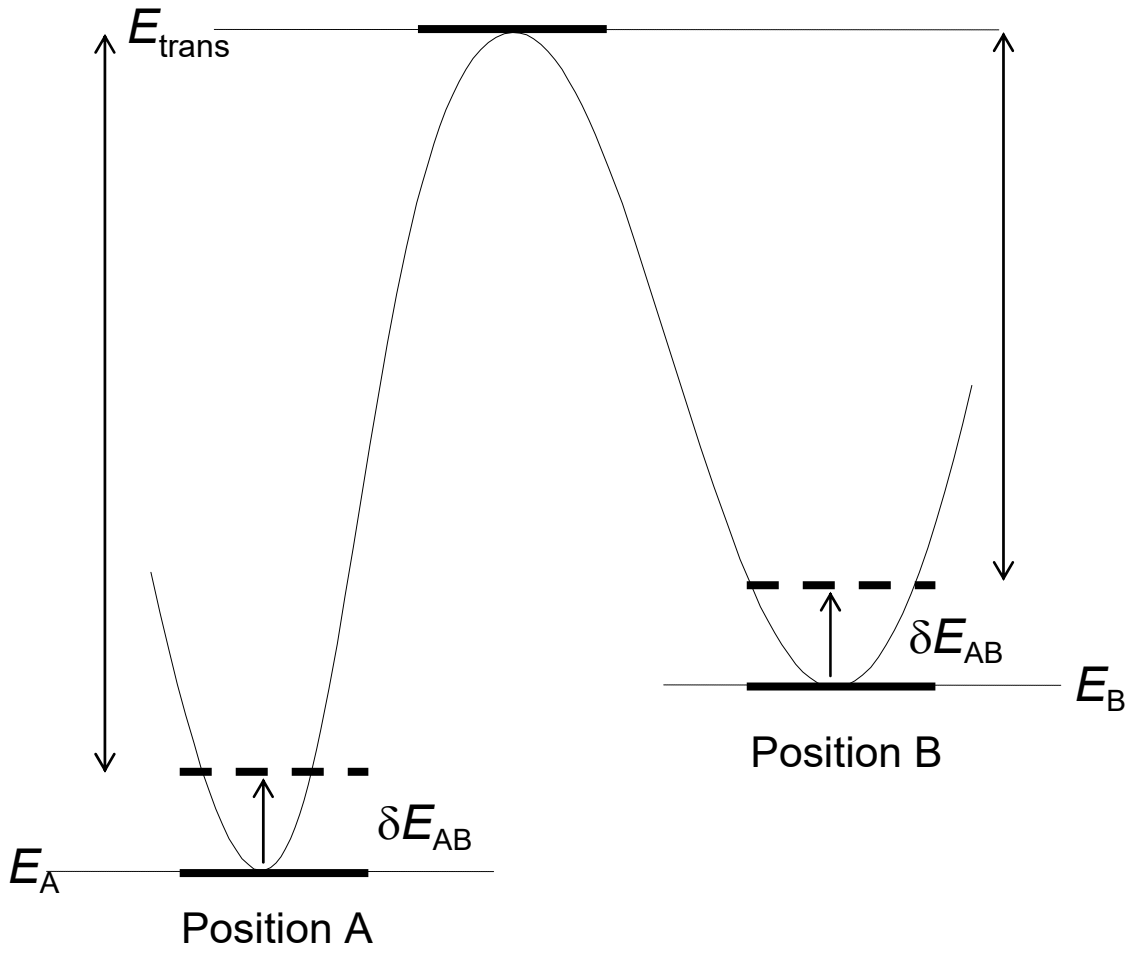

Figure S14. Energy scheme used for KMC simulations used here. Two particles adsorbed at adjacent sites experience a repulsive interaction energy $\delta E_{\alpha\beta}$.

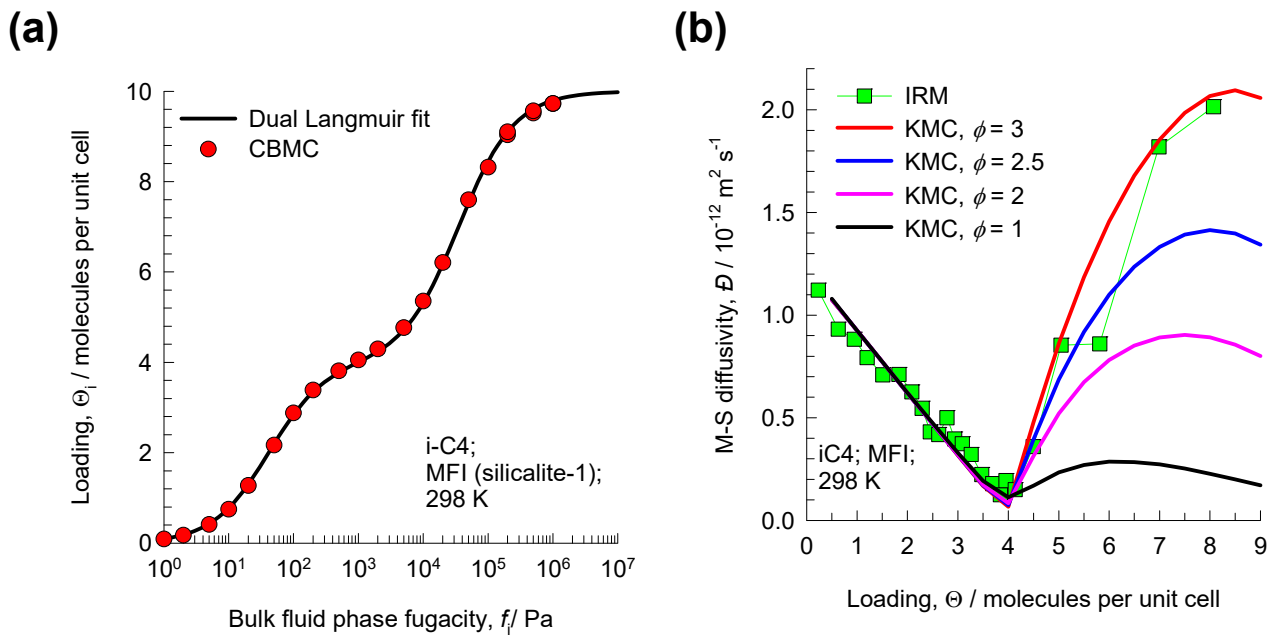

Figure S15. (a) CBMC simulations of the iC4 isotherm in MFI zeolite at 298 K. The continuous solid lines are the dual-site Langmuir fits using the parameter values specified in Table S1. (b) Experimental data of Chmelik et al.[29] on the M-S diffusivity of iC4 in MFI zeolite at 298 K (indicated by filled symbols). The continuous solid lines are the KMC simulations with different choices of the molecule-molecule interaction parameters $\phi = 1$, 2, 2.5 and 3.

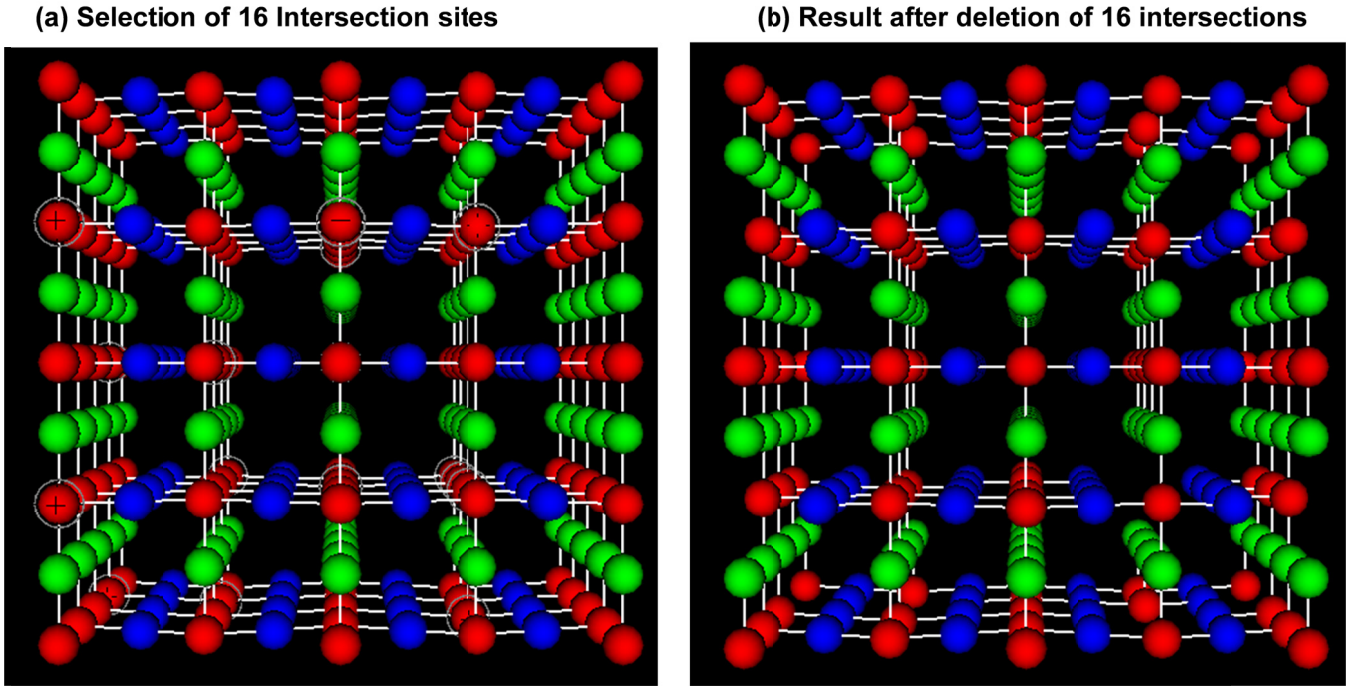

Figure S16. Pictorial illustration of strategy for (a) random selection of 16 intersection sites, and (b) resulting super cell after deletion of 16 interesection sites.

Kinetic Monte Carlo (KMC) simulations

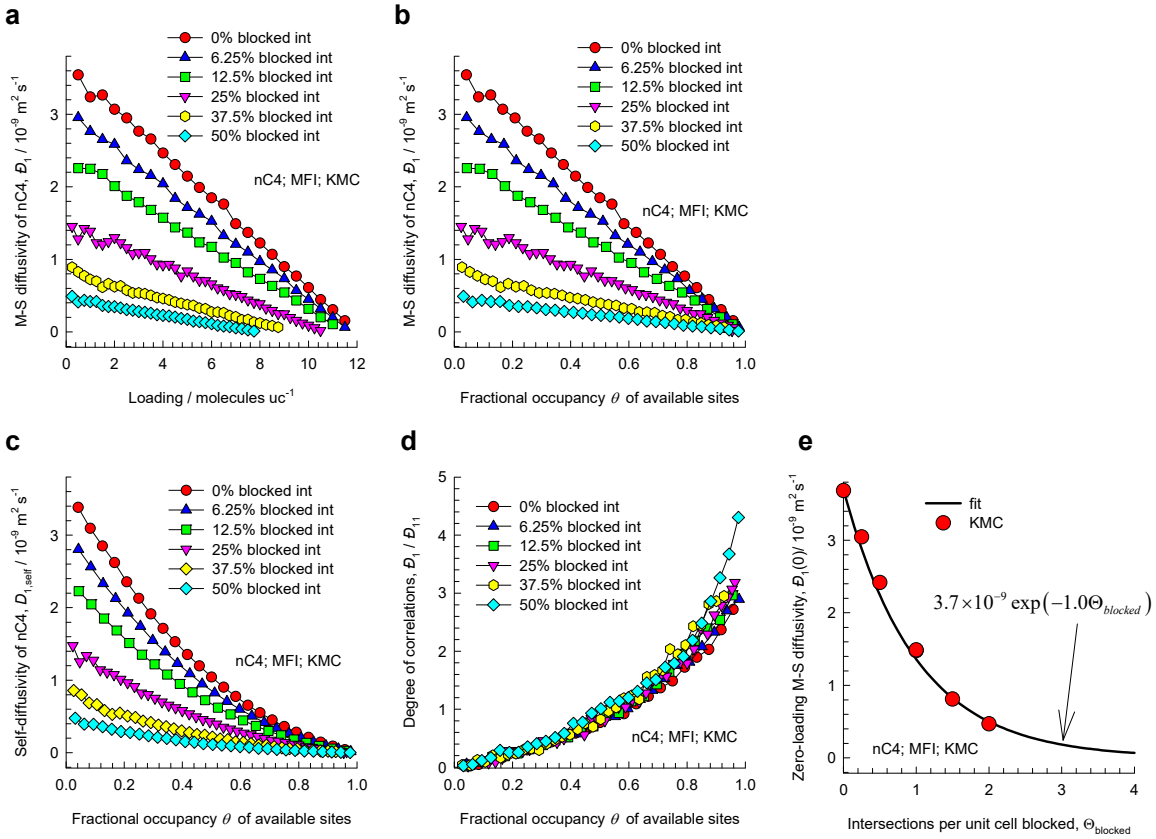

Figure S17. (a, b, c, d) KMC simulation results for the influence of the degree of intersection blocking on M-S diffusivity, $Đ_1$, self-diffusivity, $D_{1,self}$ and degrees of correlation, $Đ_1/Đ_{11}$, for nC4 diffusion in MFI zeolite. The fractional occupancy is the total loading divided by the total number of available adsorption sites, after deletion of the selected number of intersection sites. (e) Zero-loading M-S diffusivity as a function of the number of blocked intersection sites per unit cell.

Kinetic Monte Carlo (KMC) simulations

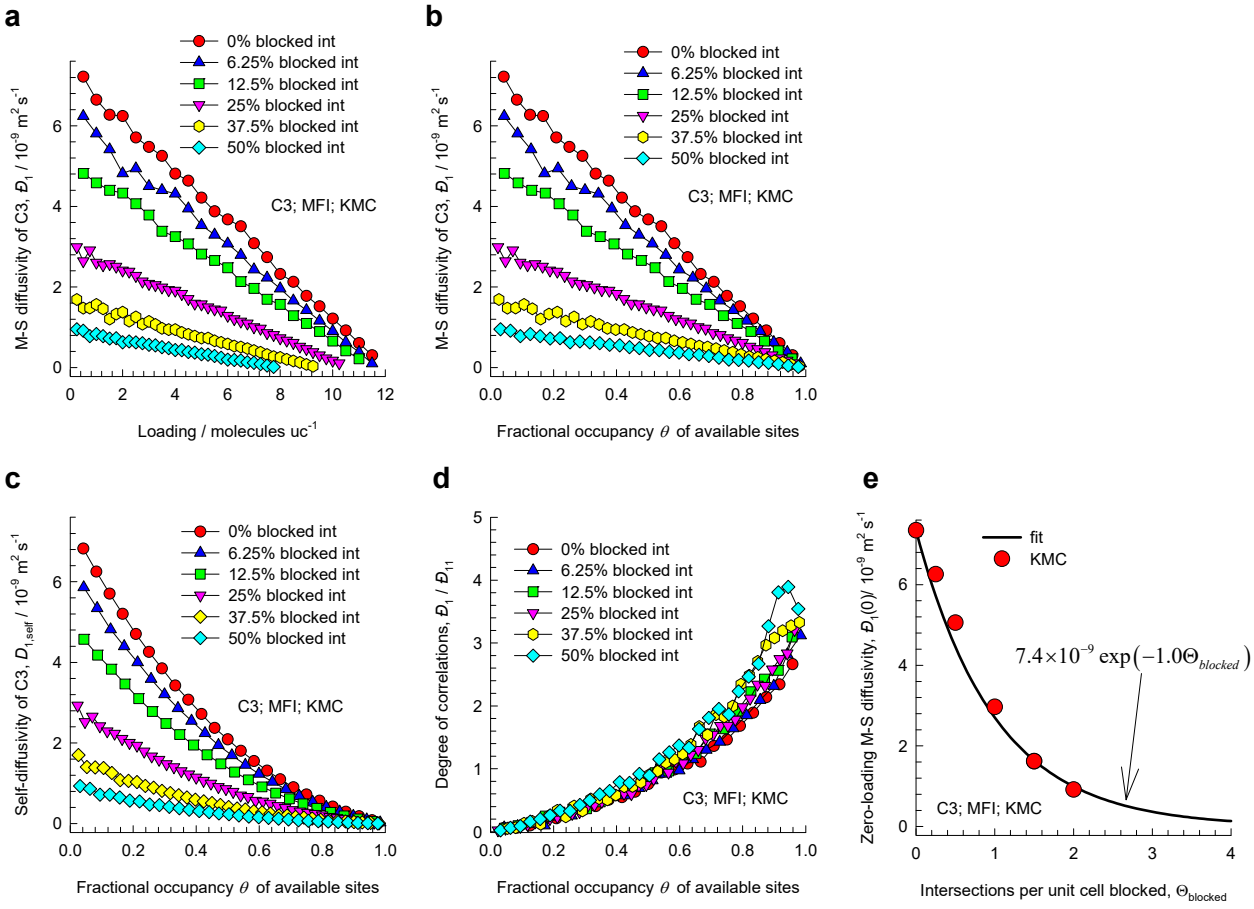

Figure S18. (a, b, c, d) KMC simulation results for the influence of the degree of intersection blocking on M-S diffusivity, $Đ_1$, self-diffusivity, $D_{1,self}$ and degrees of correlation, $Đ_1/Đ_{11}$, for C3 diffusion in MFI zeolite. The fractional occupancy is the total loading divided by the total number of available adsorption sites, after deletion of the selected number of intersection sites. (e) Zero-loading M-S diffusivity as a function of the number of blocked intersection sites per unit cell.

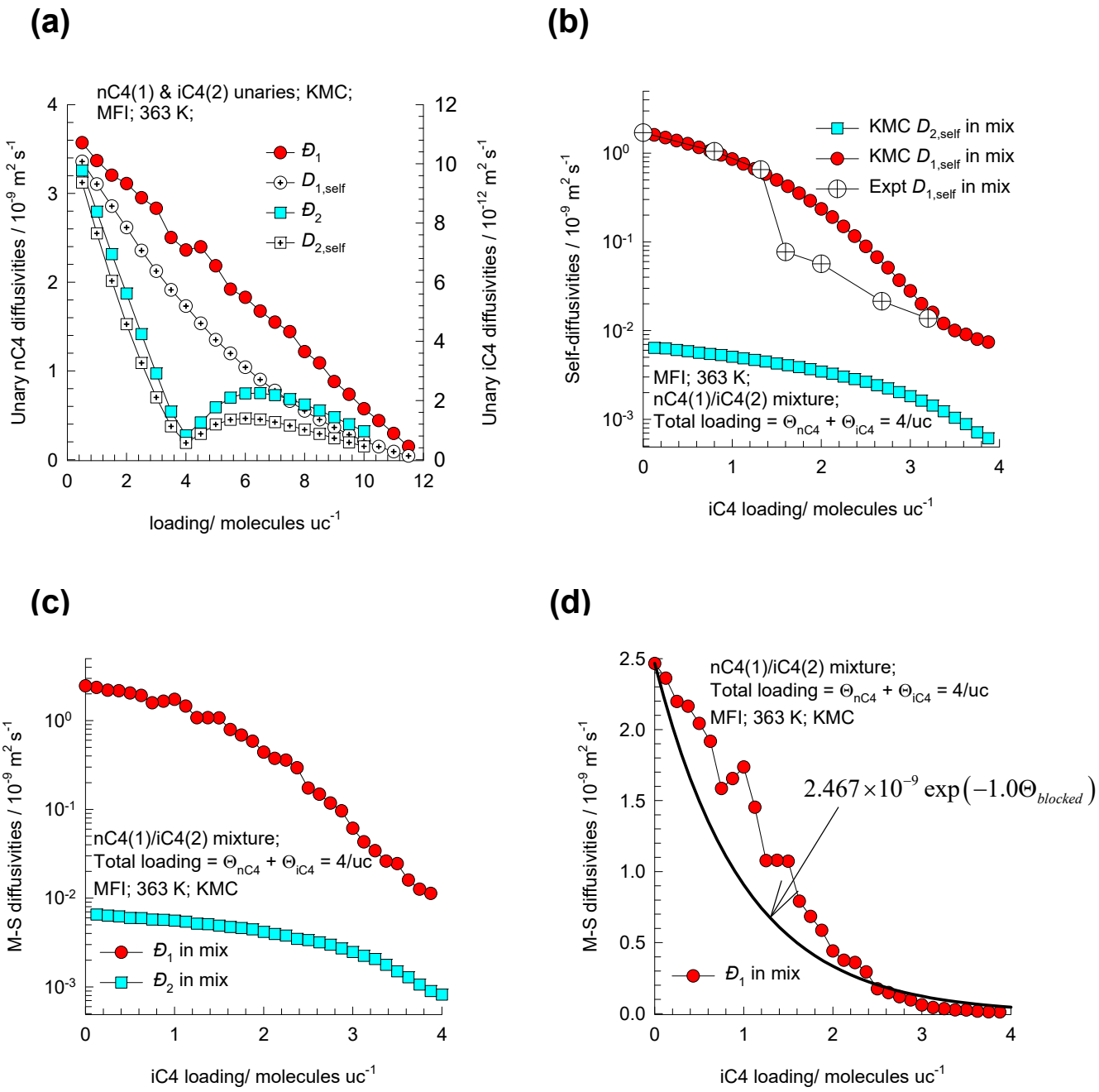

Figure S19. KMC simulation results for nC4/iC4 diffusion. (a) Unary self- and M-S diffusivities of nC4(1) and iC4(2) as a function of loading, expressed as molecules per unit cell. (b, c, d) Self- and M-S diffusivities of nC4 (1) and iC4(2) for nC4(1)/iC4(2) mixture diffusion (total loading is held constant at 4 molecules uc^{-1}), as function of the iC4 loading.

Kinetic Monte Carlo (KMC) simulations

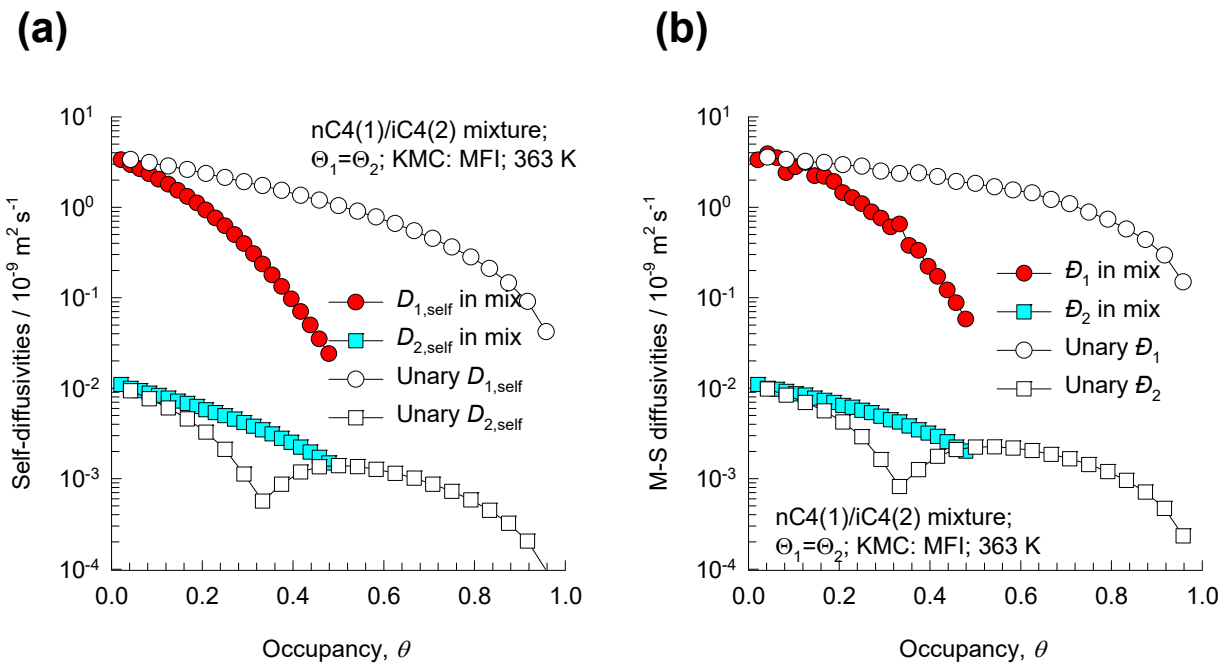

Figure S20. KMC simulations of (a) self- and (b) M-S diffusivities of nC4(1) and iC4(2) for nC4(1)/iC4(2) mixture diffusion of equimolar ($\Theta_1 = \Theta_2$) mixtures, as function of the occupancy.

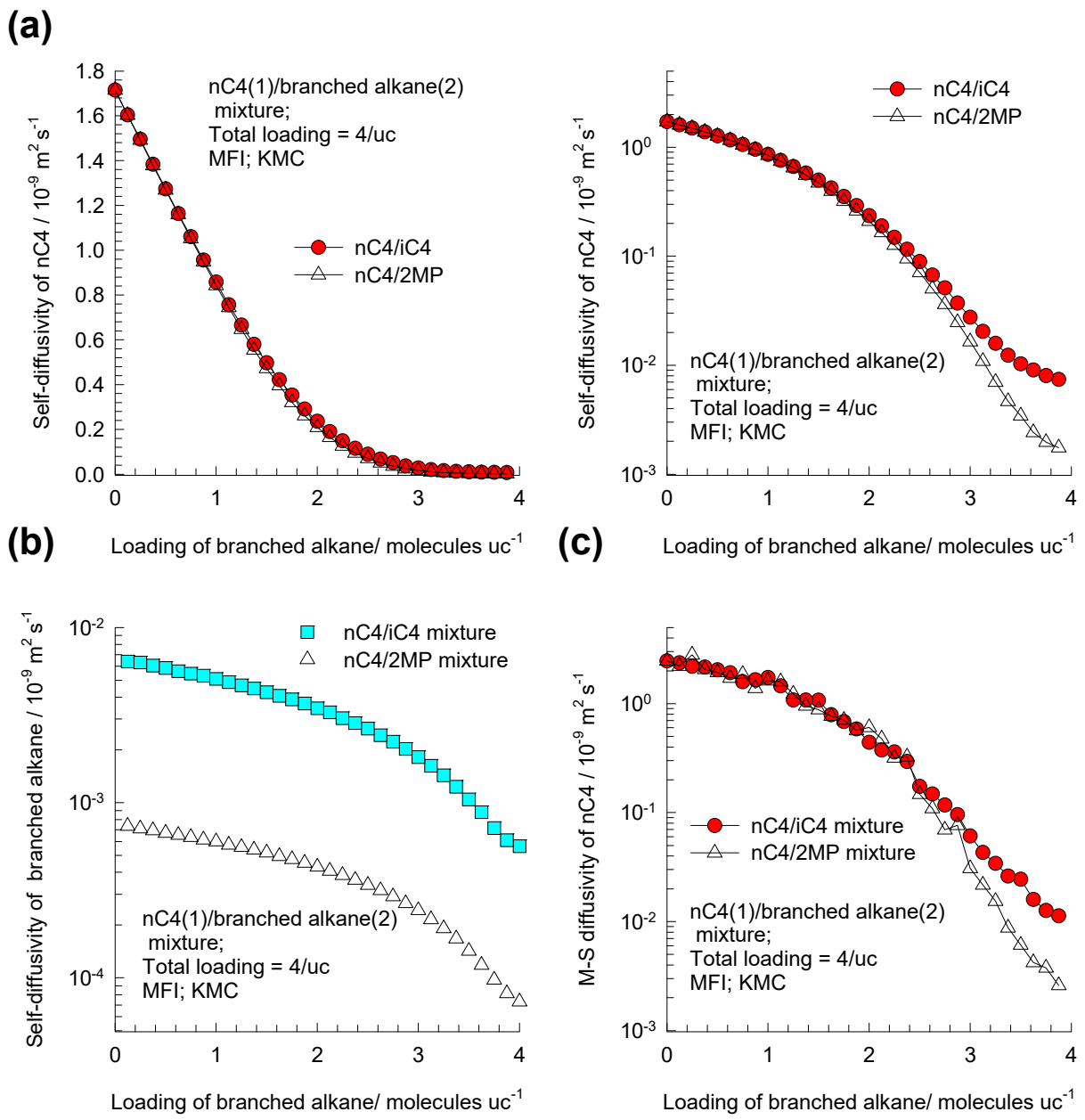

Figure S21. KMC simulation results for (a, b) self-diffusivities and (c) M-S diffusivities of nC4(1)/iC4(2) and nC4(1)/2MP(2) mixture diffusion (total loading is held constant at 4 molecules uc^{-1}), as function of the loading of the branched alkane.

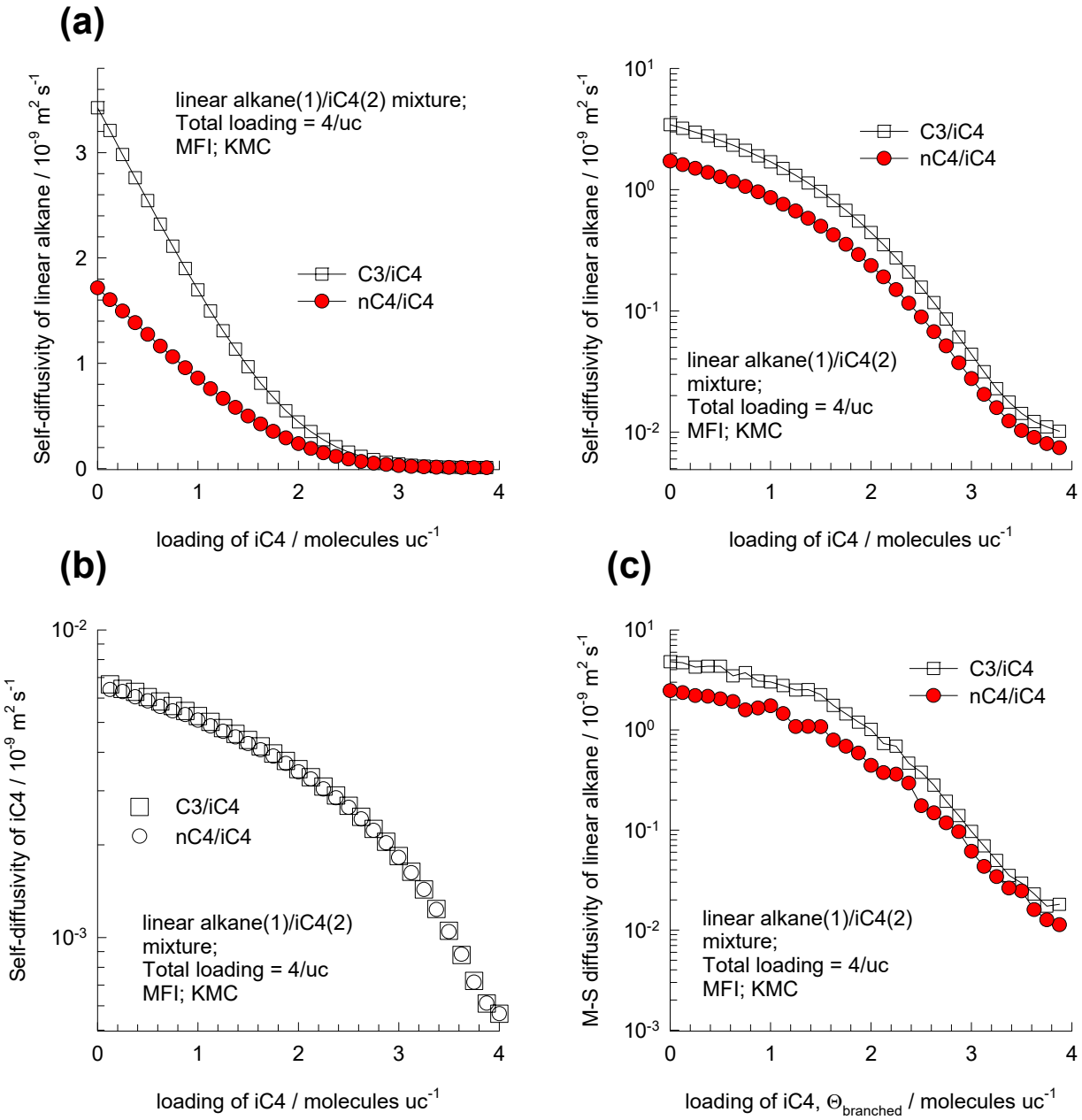

Figure S22. KMC simulation results for (a) self-diffusivities and (b, c) M-S diffusivities of nC4(1)/iC4(2) and C3(1)/iC4(2) mixture diffusion (total loading is held constant at 4 molecules uc^{-1}), as function of the loading of the iC4.

Kinetic Monte Carlo (KMC) simulations

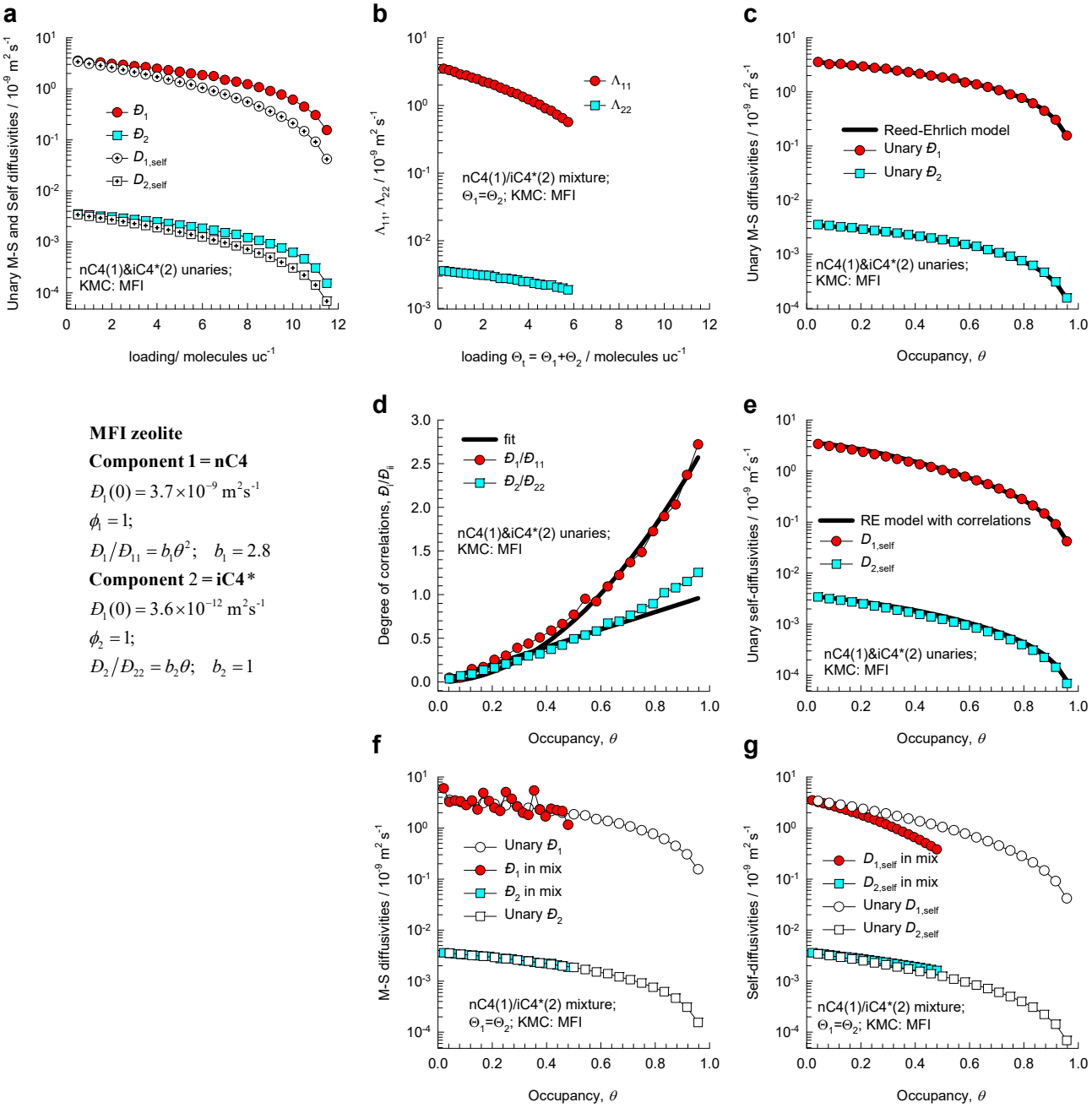

MFI zeolite

Component 1 = nC4

$Đ_1(0) = 3.7\times10^{-9}\ \mathrm{m^2 s^{-1}}$

$\phi_1 = 1;$

$Đ_1/Đ_{11} = b_1\theta^2; \quad b_1 = 2.8$

Component 2 = iC4*

$Đ_1(0) = 3.6\times10^{-12}\ \mathrm{m^2 s^{-1}}$

$\phi_2 = 1;$

$Đ_2/Đ_{22} = b_2\theta; \quad b_2 = 1$

Figure S23. KMC simulation results for nC4/(1)/iC4*(2) mixture diffusion, along with the results for unary diffusivities. (a, c, d, e) Diffusivities in unary systems. (b, f, g, h) Diffusivities in binary mixtures.

Kinetic Monte Carlo (KMC) simulations

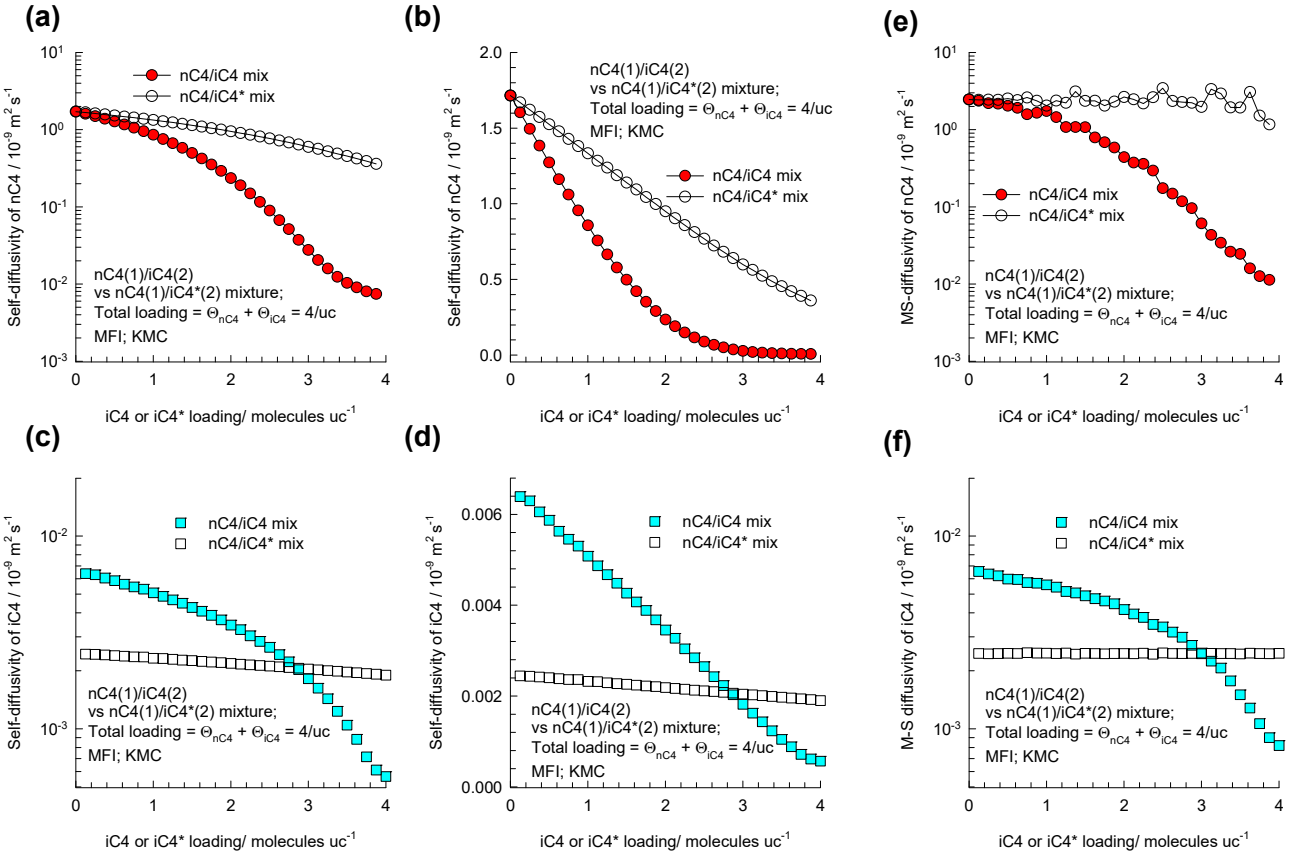

Figure S24. KMC simulation results for (a ,b, c, d) self-diffusivities, and (e, f) M-S diffusivities for nC4(1)/iC4(2) and nC4(1)/iC4*(2) mixture diffusion (total loading is held constant at 4 molecules uc^{-1}), as function of the iC4 loading. The jump frequencies of iC4 are the same used in the KMC results in Figure S19. The jump frequencies of the hypothetical iC4* towards and away from the intersections are taken to be equal to one another.

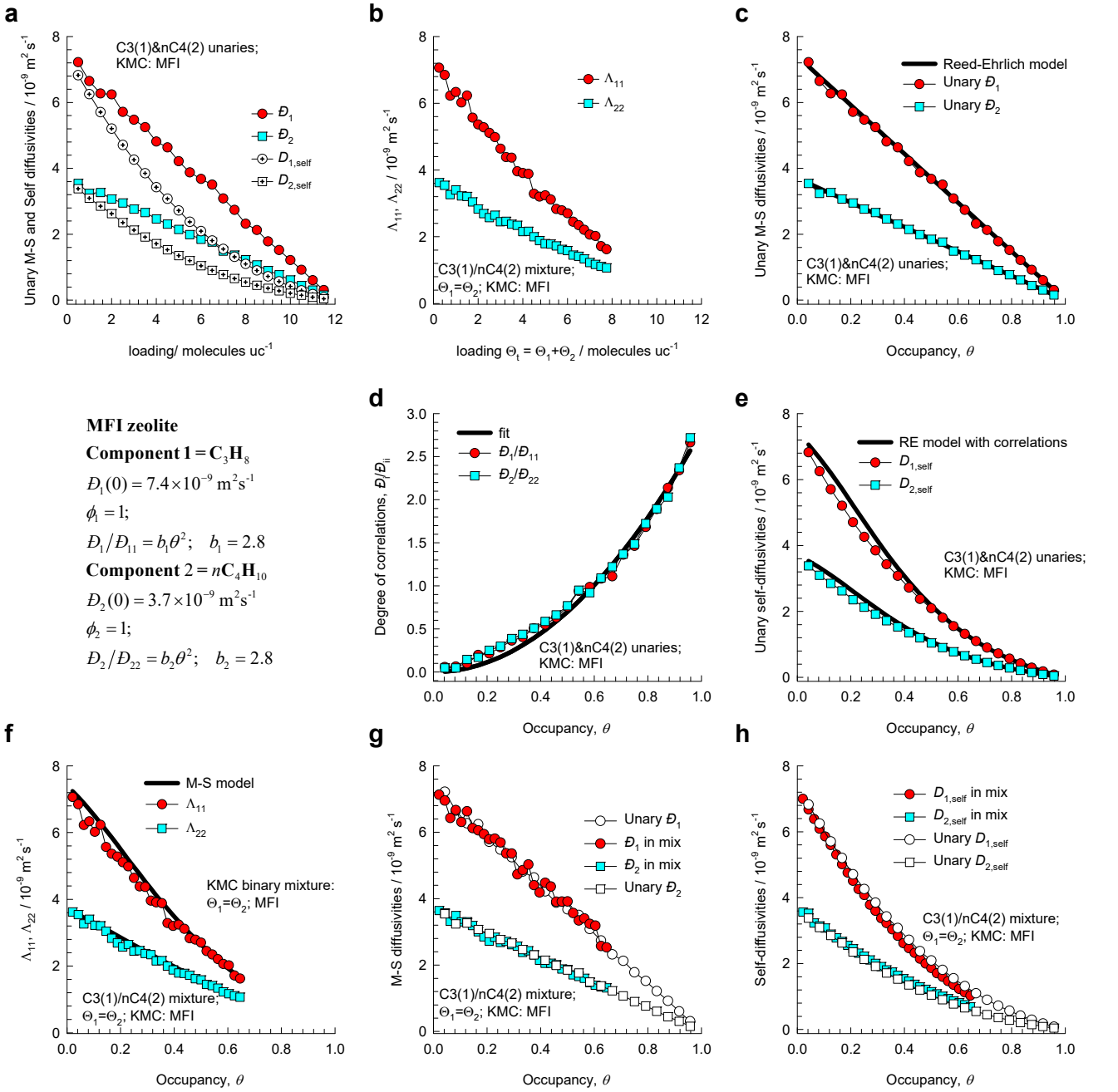

Figure S25. KMC simulation results for C3/(1)/nC4(2) mixture diffusion, along with the results for unary diffusivities. (a, c, d, e) Diffusivities in unary systems. (b, f, g, h) Diffusivities in binary mixtures.

6 Nomenclature

Latin alphabet

b_A	dual-Langmuir-Freundlich constant for species *i* at adsorption site A, $Pa^{-\nu_A}$
b_B	dual-Langmuir-Freundlich constant for species *i* at adsorption site B, $Pa^{-\nu_B}$
$[B]$	M-S matrix, m^{-2} s
$Đ_i$	Maxwell-Stefan diffusivity for molecule-wall interaction, m^2 s^{-1}
$Đ_i(0)$	M-S diffusivity at zero-loading, m^2 s^{-1}
$Đ_{ij}$	M-S exchange coefficient, m^2 s^{-1}
$Đ_{12}$	M-S exchange coefficient for binary mixture, m^2 s^{-1}
$D_{i,self}$	self-diffusivity of species *i*, m^2 s^{-1}
f	ratio of frequencies away and toward intersections, dimensionless
f_i	partial fugacity of species *i*, Pa
n	number of species in the mixture, dimensionless
n_i	number of molecules of species *i* in simulation box, dimensionless
N_i	molar flux of species *i* with respect to framework, mol m^{-2} s^{-1}
p_i	partial pressure of species *i* in mixture, Pa
p_t	total system pressure, Pa
q_i	component molar loading of species *i*, mol kg^{-1}
$q_{i,sat}$	molar loading of species *i* at saturation, mol kg^{-1}
q_t	total molar loading in mixture, mol kg^{-1}
$\mathbf{r}_{l,i}(t)$	position vector for molecule *l* of species *i* at any time *t*, m

Nomenclature

R	gas constant, 8.314 J mol^{-1} K^{-1}
T	absolute temperature, K
w	energy of interaction; see equation (S32), J mol^{-1}
x_i	mole fraction of species i in adsorbed phase, dimensionless
z	distance coordinate, m

Greek alphabet

β	parameter defined in equation (S32), dimensionless
Γ_{ij}	thermodynamic factors, dimensionless
$[\Gamma]$	matrix of thermodynamic factors, dimensionless
δ_{ij}	Kronecker delta, dimensionless
ε	fractional pore volume of particle, dimensionless
ζ	coordination number defined in equation (S31), dimensionless
λ	jump distance in lattice model, m
$[\Lambda]$	matrix of Maxwell-Stefan diffusivities, m^2 s^{-1}
μ_i	molar chemical potential of component i, J mol^{-1}
π	spreading pressure, N m^{-1}
θ	fractional occupancy, dimensionless
Θ_i	loading of species i, molecules per unit cell
$\Theta_{i,sat}$	saturation loading of species i, molecules per unit cell
Θ_t	total mixture loading, molecules per unit cage, or per unit cell
ν	jump frequency, s^{-1}
ν	exponent in dual-Langmuir-Freundlich isotherm, dimensionless
ϕ	parameter defined in equation (S32), dimensionless
ρ	framework density, kg m^{-3}

Nomenclature

Subscripts

1	referring to component 1
2	referring to component 2
i	referring to component *i*
t	referring to total mixture
sat	referring to saturation conditions
V	vacancy

7 References

(1) Baerlocher, C.; McCusker, L. B. Database of Zeolite Structures. http://www.iza-structure.org/databases/, International Zeolite Association, 10 January 2002.

(2) Krishna, R. Diffusion in Porous Crystalline Materials. *Chem. Soc. Rev.* **2012**, *41*, 3099-3118.

(3) Fernandez, M.; Kärger, J.; Freude, D.; Pampel, A.; van Baten, J. M.; Krishna, R. Mixture Diffusion in Zeolites Studied by MAS PFG NMR and Molecular Simulation. *Microporous Mesoporous Mater.* **2007**, *105*, 124-131.

(4) Chmelik, C.; Heinke, L.; van Baten, J. M.; Krishna, R. Diffusion of *n*-butane/*iso*-butane Mixtures in Silicalite-1 Investigated Using Infrared (IR) Microscopy. *Microporous Mesoporous Mater.* **2009**, *125*, 11-16.

(5) Förste, C.; Germanus, A.; Kärger, J.; Pfeifer, H.; Caro, J.; Pilz, W.; Zikánóvá, A. Molecular Mobility of Methane Adsorbed in ZSM-5 Containing Co-adsorbed Benzene, and the Location of Benzene Molecules. *J. Chem. Soc., Faraday Trans. 1.* **1987**, *83*, 2301-2309.

(6) Schuring, D.; Koriabkina, A. O.; de Jong, A. M.; Smit, B.; van Santen, R. A. Adsorption and Diffusion of n-hexane/2-methylpentane Mixtures in Zeolite Silicalite: Experiments and Modeling. *J. Phys. Chem. B* **2001**, *105*, 7690-7698.

(7) Koriabkina, A. O.; de Jong, A. M.; Schuring, D.; van Grondelle, J.; van Santen, R. A. Influence of the acid sites on the intracrystalline diffusion of hexanes and their mixtures within MFI-zeolites. *J. Phys. Chem. B* **2002**, *106*, 9559-9566.

(8) Titze, T.; Chmelik, C.; Kärger, J.; van Baten, J. M.; Krishna, R. Uncommon Synergy Between Adsorption and Diffusion of Hexane Isomer Mixtures in MFI Zeolite Induced by Configurational Entropy Effects *J. Phys. Chem. C* **2014**, *118*, 2660-2665.

(9) Skoulidas, A. I.; Sholl, D. S.; Krishna, R. Correlation effects in diffusion of CH_4/CF_4 mixtures in MFI zeolite. A study linking MD simulations with the Maxwell-Stefan formulation. *Langmuir* **2003**, *19*, 7977-7988.

(10) Chempath, S.; Krishna, R.; Snurr, R. Q. Nonequilibrium MD simulations of difusion of binary mixtures containing short n-alkanes in faujasite. *J. Phys. Chem. B* **2004**, *108*, 13481-13491.

(11) Krishna, R. Describing the Diffusion of Guest Molecules inside Porous Structures. *J. Phys. Chem. C* **2009**, *113*, 19756-19781.

(12) Krishna, R.; van Baten, J. M. Onsager coefficients for binary mixture diffusion in nanopores. *Chem. Eng. Sci.* **2008**, *63*, 3120-3140.

(13) Hansen, N.; Keil, F. J. Multiscale modeling of reaction and diffusion in zeolites: from the molecular level to the reactor. *Soft Mater.* **2012**, *10*, 179-201.

(14) Krishna, R.; van Baten, J. M. An Investigation of the Characteristics of Maxwell-Stefan Diffusivities of Binary Mixtures in Silica Nanopores. *Chem. Eng. Sci.* **2009**, *64*, 870-882.

(15) Krishna, R.; van Baten, J. M. Unified Maxwell-Stefan Description of Binary Mixture Diffusion in Micro- and Meso- Porous Materials. *Chem. Eng. Sci.* **2009**, *64*, 3159-3178.

(16) Myers, A. L.; Prausnitz, J. M. Thermodynamics of Mixed Gas Adsorption. *A.I.Ch.E.J.* **1965**, *11*, 121-130.

(17) Krishna, R.; van Baten, J. M. Investigating the Influence of Diffusional Coupling on Mixture Permeation across Porous Membranes *J. Membr. Sci.* **2013**, *430*, 113-128.

(18) Krishna, R.; Baur, R. Modelling Issues in Zeolite Based Separation Processes. *Sep. Purif. Technol.* **2003**, *33*, 213-254.

References

(19) Krishna, R. The Maxwell-Stefan Description of Mixture Permeation across Nanoporous Graphene Membranes. *Chem. Eng. Res. Des.* **2018**, *133*, 316-325. https://doi.org/10.1016/j.cherd.2018.03.033.

(20) Reed, D. A.; Ehrlich, G. Surface diffusion, atomic jump rates and thermodynamics. *Surf. Sci.* **1981**, *102*, 588-609.

(21) Krishna, R.; Paschek, D.; Baur, R. Modelling the occupancy dependence of diffusivities in zeolites. *Microporous Mesoporous Mater.* **2004**, *76*, 233-246.

(22) Krishna, R.; van Baten, J. M. A molecular dynamics investigation of a variety of influences of temperature on diffusion in zeolites. *Microporous Mesoporous Mater.* **2009**, *125*, 126-134.

(23) Paschek, D.; Krishna, R. Monte Carlo simulations of self- and transport-diffusivities of 2-methylhexane in silicalite. *Phys. Chem. Chem. Phys.* **2000**, *2*, 2389-2394.

(24) Paschek, D.; Krishna, R. Diffusion of binary mixtures in zeolites: Kinetic Monte Carlo versus molecular dynamics simulations. *Langmuir* **2001**, *17*, 247-254.

(25) Paschek, D.; Krishna, R. Monte Carlo simulations of sorption and diffusion of isobutane in silicalite. *Chem. Phys. Lett.* **2001**, *342*, 148-154.

(26) Krishna, R.; van Baten, J. M.; Dubbeldam, D. On the Inflection in the Concentration Dependence of the Maxwell-Stefan diffusivity of CF_4 in MFI zeolite. *J. Phys. Chem. B* **2004**, *108*, 14820-14822.

(27) Krishna, R.; van Baten, J. M. Kinetic Monte Carlo simulations of the loading dependence of diffusion in zeolites. *Chem. Eng. Technol.* **2005**, *28*, 160-167.

(28) Krishna, R.; Paschek, D. Verification of the Maxwell-Stefan theory for tracer diffusion in zeolites. *Chem. Eng. J.* **2002**, *85*, 7-15.

(29) Chmelik, C.; Heinke, L.; Kärger, J.; Shah, D. B.; Schmidt, W.; van Baten, J. M.; Krishna, R. Inflection in the Loading Dependence of the Maxwell-Stefan Diffusivity of Iso-butane in MFI Zeolite. *Chem. Phys. Lett.* **2008**, *459*, 141-145.

(30) Ferreira, A. F. P.; Mittelmeijer-Hazeleger, M. C.; Bliek, A. Adsorption and differential heats of adsorption of normal and *iso*-butane on zeolite MFI. *Microporous Mesoporous Mater.* **2006**, *91*, 47-52.

(31) Auerbach, S. M. Theory and simulation of jump dynamics, diffusion and phase equilibrium in nanopores. *Int. Rev. Phys. Chem.* **2000**, *19*, 155-198.

(32) Coppens, M. O.; Bell, A. T.; Chakraborty, A. K. Dynamic Monte-Carlo and mean-field study of the effect of strong adsorption sites on self-diffusion in zeolites. *Chem. Eng. Sci.* **1999**, *54*, 3455-3463.

(33) Paschek, D.; Krishna, R. Kinetic Monte Carlo simulations of transport diffusivities of binary mixtures in zeolites. *Phys. Chem. Chem. Phys.* **2001**, *3*, 3185-3191.

(34) Paschek, D.; Krishna, R. Inter-relation between self- and jump-diffusivities in zeolites. *Chem. Phys. Lett.* **2001**, *333*, 278-284.

(35) Krishna, R. Occupancy Dependency of Maxwell−Stefan Diffusivities in Ordered Crystalline Microporous Materials. *ACS Omega* **2018**, *3*, 15743-15753. https://doi.org/10.1021/acsomega.8b02465.

(36) Krishna, R.; van Baten, J. M. Investigating the Relative Influences of Molecular Dimensions and Binding Energies on Diffusivities of Guest Species Inside Nanoporous Crystalline Materials *J. Phys. Chem. C* **2012**, *116*, 23556-23568.

(37) Krishna, R.; van Baten, J. M. Influence of Adsorption Thermodynamics on Guest Diffusivities in Nanoporous Crystalline Materials. *Phys. Chem. Chem. Phys.* **2013**, *15*, 7994-8016.

(38) Krishna, R.; van Baten, J. M. Diffusion of Hydrocarbon Mixtures in MFI Zeolite: Influence of Intersection Blocking. *Chem. Eng. J.* **2008**, *140*, 614-620.